Integration of Transparent Insulation Materials into Solar Collector Devices

Julian D. Osorio[1], Alejandro Rivera-Alvarez[2], Philibert Girurugwiro[3], Sam Yang[4], Rob Hovsapian[5] Juan C. Ordonez[6]

[1]jdo12@fsu.edu, [2]rivera@caps.fsu.edu

[3] girurugwiro@caps.fsu.edu, [4]syang6@fsu.edu

[5]rob.hovsapian@inl.gov, [6]ordonez@caps.fsu.edu

[1,2,3,4,6]Department of Mechanical Engineering, Energy and Sustainability Center, Center for Advanced Power Systems, Florida State University, Tallahassee, FL 32310, USA

[1,5]Idaho National Laboratory, Idaho Falls, ID 83402, USA

Abstract

The integration of Transparent Insulation Materials (TIMs) into Flat Plate Collectors (FPCs), Parabolic Trough Collectors (PTCs), and Central Receiver (CR) collectors is studied in this paper. A general model consisting in optical and thermal analyses is developed. At low absorber temperatures the performance of traditional collectors is slightly superior. At higher temperatures, instead, the efficiency of these collectors reduces dramatically due to the increment of heat losses. The incorporation of a TIM decreases thermal losses, leading to higher collectors' efficiencies at high absorber temperatures. The effects of TIM's properties, such as emittance, thermal conductivity, extinction coefficient, and thickness, on the collectors' performance, are also analyzed. In general, TIMs, for high performance collectors, are characterized by low emittances and thermal conductivities, high transmittances, and low extinction coefficients. The effect of the concentration ratio, for CRs and PTCs, is also analyzed in this paper. High efficiencies can be reached in conventional solar collectors having large concentration ratios. In this work, the integration of a TIM into CRs and PTCs leads to a high efficiency, even at low concentration ratios.

Keywords: Transparent Insulation Material (TIM), Flat Plate Collector (FPC), Parabolic Trough Collector (PTC), Central Receiver (CR), Efficiency, Thermal Losses

Nomenclature

		subscripts	
T	Temperature, (K)		
q_{ab}	Energy absorbed, (kW)	FPC	Flat plate collector
q_{loss}	Energy losses, (kW)	PTC	Parabolic trough collector
I_r	Peak direct-normal radiation, (W/m^2)	CR	Central receiver
h	Convection heat transfer coefficient, (W/m^2-K)	HTF	Heat transfer fluid
k	Thermal conductivity, (W/m-K)	GE	Glass envelope
R	Thermal resistance, (K/W)	TIM	Transparent insulation material
H	Height, (m)	ab	Absorber
D	Diameter, (m)	cf	Collector field
L	Length, (m)	env	Environment
t	Radius or thickness, (mm)	Sky	Sky
σ	Stefan–Boltzmann constant, (W/m^2-K^4)	$loss$	Losses
α	Absorber solar absorptance	cd	Conduction
R_{ra}	Reflected radiation, (%)	cv	Convection
μ	TIM's Extinction coefficient, (m^{-1})	r	Radiation
τ_s	Glass envelope's transmittance	tot	Total
ε	Thermal emittance	lim	limit
C	Concentration ratio	0	Reference condition
η	Efficiency, (%)	c	Collection

1. Introduction

Renewable-based technologies are becoming fundamental alternatives for energy conversion and power generation. The use of these technologies can mitigate the environmental impact caused by the extensive use of fossil fuels. Among renewables resources, solar energy is, probably, the most promising alternative to satisfy the rising energy demand. In fact, the concentrated solar power generation potential is more than hundred times the total energy consumed in the world [1]. The solar radiation can be directly collected and converted into thermal energy for water and space heating using Flat Plate Collectors (FPC). These types of collectors, traditionally, consist of a multilayer system composed of absorber elements, such as tubes, plates or channels, where the solar energy is converted into heat and then transferred to a working fluid. In FPC, the absorber is located between a transparent cover (glass envelope) and a backing insulation layer to reduce heat losses. Operating temperatures of between 80°C and 120°C can be achieved with this type of collector using water as working fluid [2]. Higher temperatures can be accomplished by concentrating the solar energy. Concentrated solar power (CSP) technologies use a solar receiver located in a focal point or focal line, where the energy is concentrated after reflection processes. Two of the main CSP technologies are the Parabolic Trough Collector (PTC) and the Central Receiver (CR) collector also known as solar tower. The temperatures

reached with these collectors allow the system to operate in conjunction with modified Brayton or Rankine power generation cycles driven by solar energy.

PTC systems have been successfully used in commercial applications [3]. They consist of an absorber, usually a metallic tube, where the energy is transferred to a working fluid, a concentric glass envelope, an annular air gap or vacuum to reduce heat losses, and a solar tracking mechanism. The geometrical concentration ratio for these systems usually varies from 15 to 45 [4]. Working fluids, such as water, oil and organic compounds, are typically used for operating temperatures of between 100°C and 400°C [5]. PTC plants can operate with Brayton or Rankine cycles [6-8]; however, it has been found that good efficiencies are achieved in these systems operating in Rankine cycles for temperatures lower than 500°C [6, 7]. PTCs can generate vapor directly to be used in a power cycle, and also, they can heat thermal oil or organic fluids to generate vapor indirectly in a heat exchanger [5]. Higher operating temperatures and power generation capacities can be obtained using CR collectors. In this configuration, the solar receiver operates at high temperatures, and under non-uniform solar radiation and environmental conditions. This operation requires special materials being able to withstand thermal stresses, corrosion and fatigue at high temperatures. This component has a strong effect on the system performance, and, together with the heliostats, represents about 50% to 70% of the total cost of the plant [9, 10]. Two types of receivers for solar tower systems are commonly used: external and cavity receivers. The first type consists of a series of panels of tubes arranged in a cylindrical layout. Usually, darkened metal tubes have been used with steam and molten salt for operating temperatures of between 500°C and 600°C; higher temperatures, of up to 900°C, are possible for tubular receiver operating with gas [11]. Cavity receivers, on the other hand, have the absorbing surface or volume inside of an insulated compartment to provide some level of insulation with the surroundings. Both types of receivers can be designed to collect solar energy in a surface or volume by using porous materials resistant to high temperatures. Usually, external receivers operate at higher temperatures and the heliostat field can be accommodated around the tower. On the other hand, the insulation in cavity receivers can lead to higher efficiencies due to lower heat losses; however, its geometry restricts the accommodation of the heliostats in a portion of azimuthal angles [12].

In general, higher operating temperatures in solar collectors lead to larger cycle efficiencies, but also increase thermal losses that reduce the collection efficiency. This situation represents a great potential for improvement of solar collectors via design optimization. Numerous experimental and theoretical studies have been done in FPCs [13-16], PTCs [17-20] and CR collectors [21-25], trying to

reach such a goal. Most of them are focused on modelling and calculating thermal losses, as well as optimizing and analyzing the effects of operating and design parameters on the solar collector's efficiency and performance for specific applications. Improvements over these components are usually based on the reduction of energy losses and/or increment in the heat transfer to the working fluid. In particular, multi-layer glass covers and transparent insulating materials have been analyzed to reduce thermal losses in FPCs [26-29]. Also, roughened absorber plates [30], as well as internal fins with rectangular and triangular shapes inside the channels or tubes [26, 31, 32], have been proposed in order to increase the heat transfer coefficient by increasing the effective heat transfer area, and by inducing turbulence in the working fluid. The use of fins inside and outside FPCs has shown favorable results in the enhancement of the heat transfer coefficient, leading to significant improvements in the collector's efficiency [26, 31-33]. The fin shape optimization based on operating conditions, geometric restrictions and specific applications is fundamental to achieve additional gains in the solar collectors and heat exchangers performance [34]. In order to improve the efficiency of PTCs, some novel design changes have been proposed. Some of these changes include the addition of helical fins [35] and porous discs [36] inside the absorber, a reduction in diameter of the absorber tube to decrease the thermal resistance by inducing a turbulent regime in the fluid, and the incorporation of external fins to keep the area of the absorber constant while improving the heat transfer coefficient [32]. Significant progress in the performance of solar plants has been accomplished using selective coatings on the absorber due to an increment in the solar absorptance, and a reduction in the thermal emittance [37]. Similarly, in CR collectors, remarkable improvements in the efficiency have been accomplished by implementing different designs, including tubes with dimpling and induced roughness [38, 39], spiral tubes [40], hexagonal pyramidal elements [41], and multi-diameter tubes [42]. Different materials for tubes, such as stainless steels and nickel alloys, coatings and glasses, have also been tested to reduce heat losses [43-46]. In addition, the performance of a wide variety of heat transfer and working fluids have been assessed [44], as well as porous materials inside the tube [47], and suspended particles in the working fluid to enhance the heat transfer coefficient [48].

Thermal insulation is an essential alternative to reduce heat losses and enhance the performance of any thermal component or system. The fast development of solar-based energy conversion devices, where solar collectors emerge as key components, has ignited the demand of more efficient devices, with materials capable of operating at high temperatures while being resistant to corrosion, fracture and fatigue. Transparent insulation materials (TIMs), from products like polymer

sheets, capillaries and cellular profiles, have been broadly investigated to be used as effective thermal insulators in solar energy applications [27, 28, 46, 49-51]. In this work, the effect of the integration of transparent insulation materials on the performance of solar collectors' receivers is investigated. A general thermal and optical model for FPCs, PTCs and CR collectors is presented. The effects of integrating a TIM, and different TIM's properties, on the performance of these collectors are studied. The efficiency of the proposed designs is assessed and compared with that of traditional solar collector configurations. TIMs have been successfully used in FPCs to allow higher operating temperatures and reduce energy losses [2, 27-29]. These materials are transparent to solar radiation wavelengths while providing good thermal insulation and restricting infrared energy losses via re-radiation [49]. Some models to evaluate different arrangements of square-cell honeycomb TIMs in FPCs have been done [50, 51]. In general, increments in the efficiency of between 7% and 12% in this type of collector, using TIMs, have been reported [52, 53]. Besides FPC, and some isolated works about the TIM integration in cavity central receivers [54], applications of TIMs in PTCs and external CR collectors are still a subject to be developed in the literature.

2. Solar collector model

In non-concentrating solar devices, such as flat plate collectors, the solar energy coming from all direction can be absorbed, i.e. direct-normal and diffuse components of solar radiation. In concentrating solar collectors, the receivers can operate under solar radiation flux concentrations of between 15 and 45 times the direct-normal radiation for PTCs, and between 100 and 1500 times for CR collectors [4]. This high concentrated energy leads the system to operate at high temperatures which favor the power cycle efficiencies, but, at the same time, can affect the efficiency of the collector due to energy losses. The incorporation of a transparent insulation material (TIM) into the three most common types of solar collectors (FPC, PTC, and CR) is studied in this paper. The addition of this component helps to reduce heat losses, allowing higher efficiencies at higher operating temperatures. Schematic designs of each of the solar collectors with a TIM integrated are presented in Fig. 1.

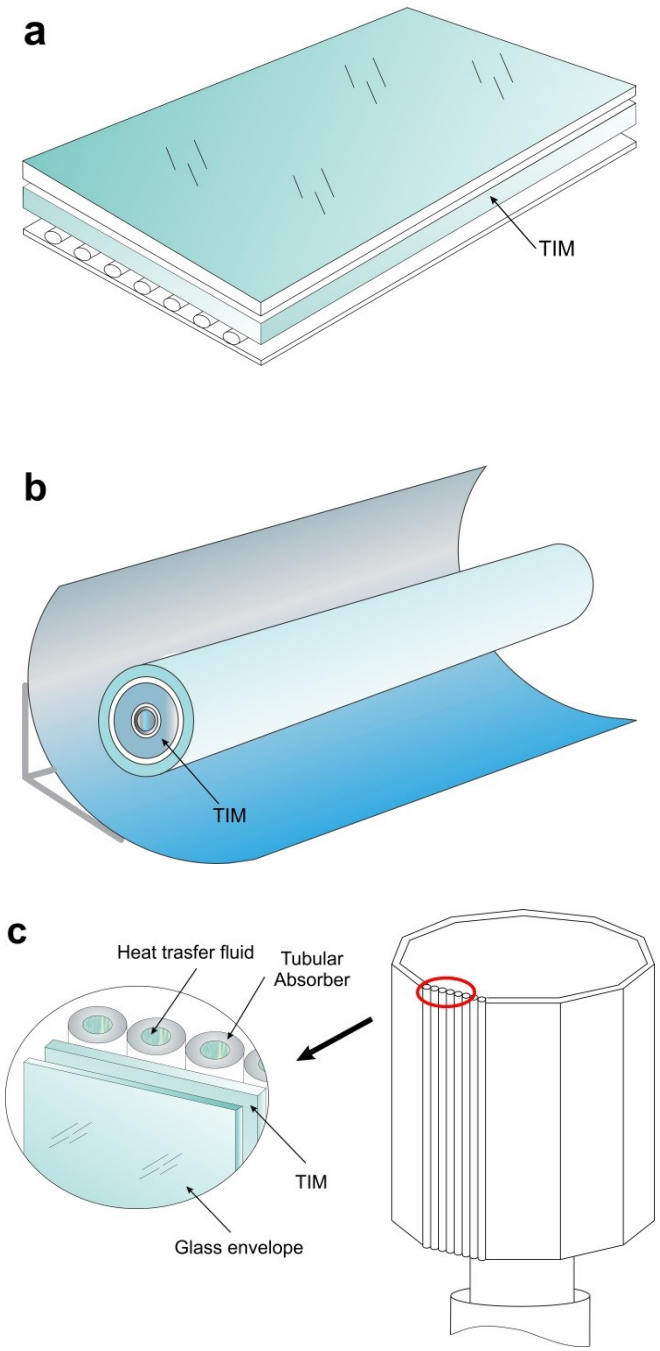

Figure 1. Schematic illustration of solar receivers including a TIM. a) FPC. b) PTC. c) CR.

In this section, a general model for solar receivers to quantify the total solar energy absorbed by the collector's absorber, and the respective thermal losses for FPCs, PTCs, and CR collectors is developed. The effects of TIM's thickness, thermal and optical properties, as well as the working fluid temperature on the collectors' performance are studied. In this model, an optical analysis taking into

account each of the collector layers is done to determine the solar energy reflection and attenuation when passing through the glass envelope (GE) and TIM. Similarly, the thermal losses are evaluated by using a thermal resistance approach. The general one-dimensional optical and thermal energy model of a solar collector's receiver with a TIM is displayed in Fig. 2.

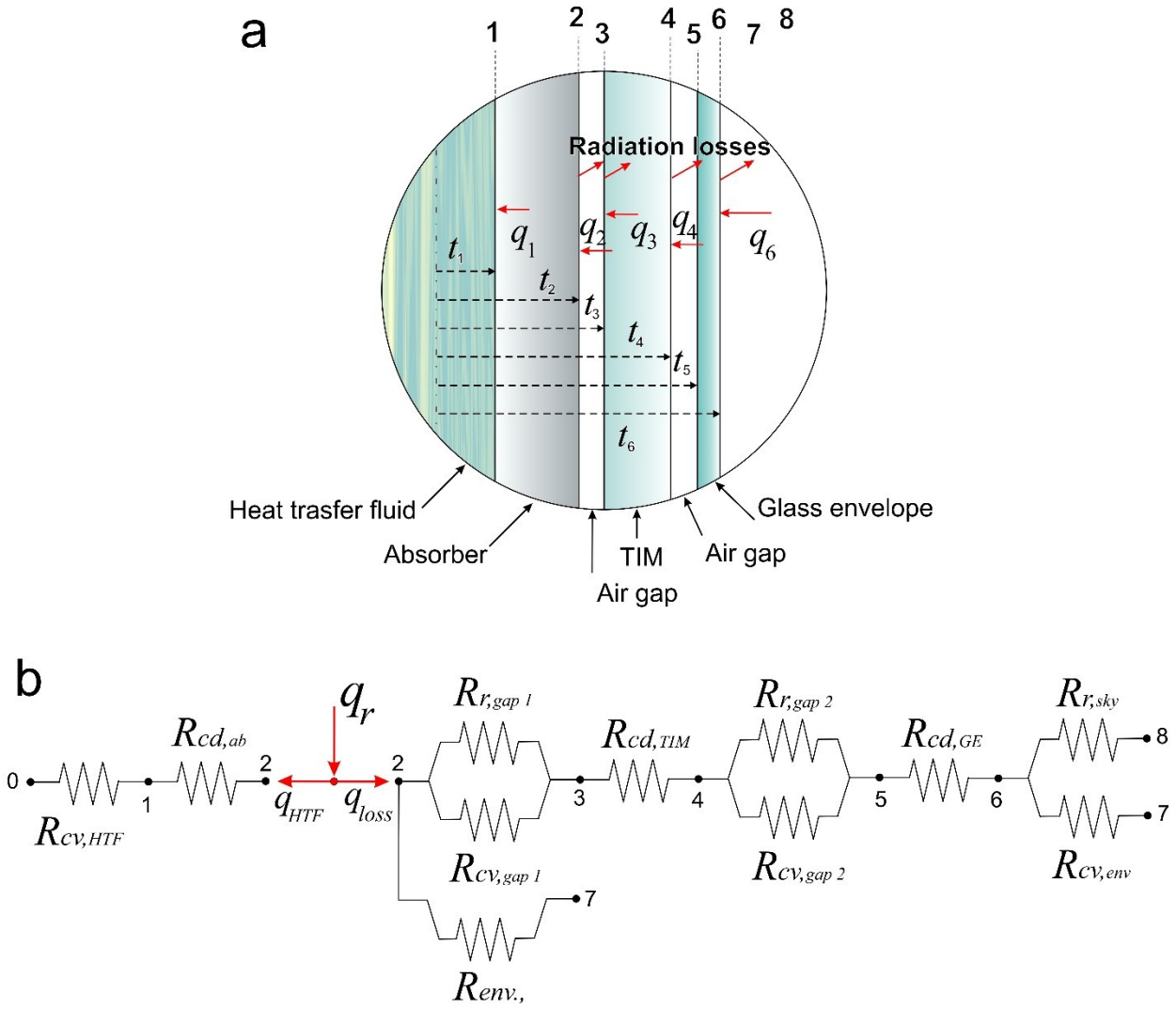

Figure 2. General energy model of a solar receiver with a TIM.

The solar energy reaching the HTF (q_{HTF}) can be calculated as the energy absorbed by the collector's absorber (q_r) minus the heat losses (q_{loss}):

$$q_{HTF} = q_r - q_{loss} \quad (1)$$

The solar radiation is attenuated and reflected in each of the layers until it reaches the absorber at point 2 (see Fig. 2a). An important amount of this energy is absorbed in the first angstroms of the absorber's surface [55], while the remaining fraction gets lost and returns back to the environment by passing through the receiver's layers (air gaps, TIM and GE), and also along the support brackets via conduction (see thermal circuit in Fig 2b.). All these losses are taken into account in the last term of Eq. 1 (q_{loss}). The remaining energy (q_{HTF}) is transferred by conduction towards the absorber's interior and reaches the HTF.

2.1. Optical analysis

The solar radiation reaching the external layer of the GE (q_6) can be determined as:

$$q_6 = I_r A_{ab} C \eta_c \quad (2)$$

Where I_r, usually taken as 1000 W/m^2, is the reference, peak, global radiation for the FPC, and the peak, direct-normal radiation for the other two collector types. A_{ab} is the irradiated projected area of the absorber, η_c is the collection efficiency (see section 3), and C is the concentration ratio.

When passing through the GE and TIM, a fraction of the radiation is reflected and attenuated by those materials (see Fig. 2a). The solar energy reaching the TIM's outer (q_4), the TIM's inner (q_3), and the absorber's outer surface (q_2) is, respectively, calculated as:

$$q_4 = q_5 = q_6 \tau_s \quad (3)$$

$$q_3 = q_4 (1 - R_{ra}) e^{-\mu(t_4 - t_3)} \quad (4)$$

$$q_2 = q_4 (1 - R_{ra})^2 e^{-\mu(t_4 - t_3)} \quad (5)$$

where τ_s is the GE's transmittance, R_{ra} is the reflected radiation, μ is the TIM's Extinction coefficient and $t_4 - t_3$ is the TIM's thickness.

Finally, the solar energy absorbed by the absorber after passing through the different solar collector's layers is determined by:

$$q_r = q_2 \alpha \tag{6}$$

where α is the absorber's solar absorptance.

A similar analysis applied over traditional solar collectors, FPC, PTC and CR without a TIM, yields:

$$q_{r_{No\,TIM}} = q_6 \tau_s \alpha \tag{7}$$

It is important to note that because the external CRs do not have a GE, τ_s will be taken as 1 in Eq. 7 when analyzing such a case.

2.2. Thermal analysis

Based on the thermal circuit presented in Fig 2b, the energy losses in the solar receiver can be determined as follows:

$$q_{loss} = (T_2 - T_7)/R_{tot} \tag{8}$$

where T_2 and T_7 are the absorber's and ambient temperature, respectively, and R_{tot} is the total effective thermal resistance for the circuit. In general, T_i represents the corresponding temperature at each position i, with $T_8 = T_7 - 11°C$ being the effective sky temperature. Usually, the difference between sky and air temperatures is between 5°C and 30°C depending on environmental conditions [56].

The energy reaching the HTF can be written in terms of the conduction resistance through the absorber's wall ($R_{cd,ab}$), the convection resistance inside the absorber ($R_{cv,HTF}$), and the HTF temperature (T_0) as follows:

$$q_{HTF} = \frac{(T_2 - T_0)}{R_{cd,ab} + R_{cv,HTF}} \tag{9}$$

The total thermal resistance (R_{tot}) is deducted from the thermal circuit (c.f. Fig. 2b) and can be computed in terms of every single resistance for each receiver's constituents as follows:

$$R_{tot} = \frac{\frac{R_{env}R_{cv,gap\ 1}R_{r,gap\ 1}}{R_{cv,gap\ 1}+R_{r,gap\ 1}}+R_{env}R_{cd,TIM}+\frac{R_{env}R_{cv,gap\ 2}R_{r,gap\ 2}}{R_{cv,gap\ 2}+R_{r,gap\ 2}}+R_{env}R_{cd,GE}+\frac{R_{env}R_{cv,env}R_{r,sky}}{R_{cv,env}+R_{r,sky}}}{R_{env}+\frac{R_{cv,gap\ 1}R_{r,gap\ 1}}{R_{cv,gap\ 1}+R_{r,gap\ 1}}+R_{cd,TIM}+\frac{R_{cv,gap\ 2}R_{r,gap\ 2}}{R_{cv,gap\ 2}+R_{r,gap\ 2}}+R_{cd,GE}+\frac{R_{cv,env}R_{r,sky}}{R_{cv,env}+R_{r,sky}}} \quad (10)$$

In turn, the total effective thermal resistance for the receiver of a FPC, PTC, and CR collector without a TIM, is determined from Eqs. 11 and 12, where the CR has been considered without GE.

$$R_{tot\ FPC\ No\ TIM} = R_{tot\ PTC\ No\ TIM} = \frac{R_{cv,gap}R_{rgap}R_{env}}{R_{cv,gap}R_{env}+R_{r,gap}R_{env}+R_{cv,gap}R_{r,gap}} + R_{cd,GE} + \frac{R_{cv,env}R_{r,sky}}{R_{cv,env}+R_{r,sky}} \quad (11)$$

$$R_{tot\ CR\ No\ TIM} = \frac{R_{cv,env}R_{r,sky}R_{env}}{R_{cv,env}R_{env}+R_{r,sky}R_{env}+R_{cv,env}R_{r,sky}} \quad (12)$$

Table 1. Thermal resistance expressions for each of the solar receiver's elements, including a TIM.

	Flat plate	Parabolic Trough	Central receiver
I_r	Global	Direct-normal	Direct-normal
$R_{cd,ab}$	$(t_2-t_1)/(LHk_{ab})$	$\ln(t_2/t_1)/(2\pi Hk_{ab})$	$\ln(t_2/t_1)/(2\pi Hk_{ab})$
$R_{cv,gap\ 1}$	$1/(LHh_{2-3})$	$1/(2\pi t_2 Hh_{2-3})$	$1/(2\pi t_2 H(1/2)h_{2-3})$
$R_{r,gap\ 1}$	$1/(LHh_{r,2-3})$	$1/(2\pi t_2 Hh_{r,2-3})$	$1/(2t_2 Hh_{r,2-3})$
R_{env}	$L_{dis}/(LHk_{dis})$	$L_{dis}/(A_{dis}k_{dis})$	$L_{dis}/(A_{dis}k_{dis})$
$R_{cd,TIM}$	$(t_4-t_3)/(LHk_{TIM})$	$\ln(t_4/t_3)/(2\pi Hk_{TIM})$	$(t_4-t_3)/(2t_2 Hk_{TIM})$
$R_{cv,gap\ 2}$	$1/(LHh_{4-5})$	$1/(2\pi t_4 Hh_{4-5})$	$1/(2t_2 Hh_{4-5})$
$R_{r,gap\ 2}$	$1/(LHh_{r,4-5})$	$1/(2\pi t_4 Hh_{r,4-5})$	$1/(2t_2 Hh_{r,4-5})$
$R_{cd,GE}$	$(t_6-t_5)/(LHk_{GE})$	$\ln(t_6/t_5)/(2\pi Hk_{GE})$	$(t_6-t_5)/(2t_2 Hk_{GE})$
$R_{cv,env}$	$1/(LHh_7)$	$1/(2\pi t_6 Hh_7)$	$1/(2t_2 Hh_7)$
$R_{r,sky}$	$1/(LHh_{r,8})$	$1/(2\pi t_6 Hh_{r,8})$	$1/(2t_2 Hh_{r,8})$

Table 2. Thermal resistance expressions for each of the traditional solar receiver's elements, without a TIM.

	Flat plate	Parabolic Trough	Central receiver
I_r	Global	Direct-normal	Direct-normal
$R_{cd,ab}$	$(t_2-t_1)/(LHk_{ab})$	$\ln(t_2/t_1)/(2\pi Hk_{ab})$	$\ln(t_2/t_1)/(2\pi Hk_{ab})$
$R_{cv,gap}$	$1/(LHh_{2-5})$	$1/(2\pi t_2 Hh_{2-5})$	-
$R_{r,gap}$	$1/(LHh_{r,2-5})$	$1/(2\pi t_2 Hh_{r,2-5})$	-
R_{env}	$L_{dis}/(LHk_{dis})$	$L_{dis}/(A_{dis}k_{dis})$	$L_{dis}/(A_{dis}k_{dis})$
$R_{cd,GE}$	$(t_6-t_5)/(LHk_{GE})$	$\ln(t_6/t_5)/(2\pi Hk_{GE})$	-
$R_{cv,env}$	$1/(LHh_7)$	$1/(2\pi t_6 Hh_7)$	$1/(2\pi t_2 H(1/2)h_7)$

$R_{r,sky}$	$1/(LHh_{r,8})$	$1/(2\pi t_6 Hh_{r,8})$	$1/(2\pi t_2 H(1/2)h_{r,2})$

Table 3. Radiation heat transfer coefficients for solar receivers with a TIM and GE.

	Flat plate	Parabolic Trough	Central receiver
$h_{r,2-3}$	$\frac{\sigma(T_2+T_3)(T_2^2+T_3^2)}{\frac{1}{\varepsilon_2}+\frac{1}{\varepsilon_3}-1}$	$\frac{\sigma(T_2+T_3)(T_2^2+T_3^2)}{\frac{1}{\varepsilon_2}+\frac{1-\varepsilon_3}{\varepsilon_3}\left(\frac{t_2}{t_3}\right)}$	$\frac{\sigma(T_2+T_3)(T_2^2+T_3^2)}{\frac{2}{\pi\varepsilon_2}+\frac{1}{\varepsilon_3}-1}$
$h_{r,4-5}$	$\frac{\sigma(T_4+T_5)(T_4^2+T_5^2)}{\frac{1}{\varepsilon_4}+\frac{1}{\varepsilon_5}-1}$	$\frac{\sigma(T_4+T_5)(T_4^2+T_5^2)}{\frac{1}{\varepsilon_4}+\frac{1-\varepsilon_5}{\varepsilon_5}\left(\frac{t_4}{t_5}\right)}$	$\frac{\sigma(T_4+T_5)(T_4^2+T_5^2)}{\frac{1}{\varepsilon_4}+\frac{1}{\varepsilon_5}-1}$
$h_{r,8}$	$\varepsilon_6\sigma(T_8+T_6)(T_8^2+T_6^2)$	$\varepsilon_6\sigma(T_8+T_6)(T_8^2+T_6^2)$	$\varepsilon_6\sigma(T_8+T_6)(T_8^2+T_6^2)$

Table 4. Radiation heat transfer coefficients for solar receivers without a TIM and GE.

	Flat plate	Parabolic Trough	Central receiver
$h_{r,2-5}$	$\frac{\sigma(T_2+T_5)(T_2^2+T_5^2)}{\frac{1}{\varepsilon_2}+\frac{1}{\varepsilon_5}-1}$	$\frac{\sigma(T_2+T_5)(T_2^2+T_5^2)}{\frac{1}{\varepsilon_2}+\frac{1-\varepsilon_5}{\varepsilon_5}\left(\frac{t_2}{t_5}\right)}$	-
$h_{r,2}$	-	-	$\varepsilon_2\sigma(T_8+T_2)(T_8^2+T_2^2)$
$h_{r,8}$	$\varepsilon_6\sigma(T_8+T_6)(T_8^2+T_6^2)$	$\varepsilon_6\sigma(T_8+T_6)(T_8^2+T_6^2)$	-

The specific thermal resistances, for each layer of the solar receivers with a TIM and without a TIM, are presented in Tables 1 and 2, respectively. k_{ab}, k_{TIM} and k_{GE} are the thermal conductivities of the absorber, the TIM and the GE. h_{2-3}, h_{4-5}, and h_{2-5} are the convection heat transfer coefficients in the air gaps, while h_7 is the convection heat transfer coefficient with the environment (see Fig. 2a). The thermal losses with the environment through support brackets are taken into account by considering a conduction resistance (R_{env}) in parallel with the resulting resistance from point 2 to points 7 and 8, see in Fig. 2b.

Expressions to determine the radiation heat transfer coefficients, $h_{r,2-3}$, $h_{r,4-5}$ and $h_{r,8}$, for the solar collector with a TIM are listed in Table 3. Radiation heat transfer coefficient, $h_{r,2-5}$, $h_{r,2}$ and $h_{r,8}$, for traditional collectors, without a TIM, are presented in Table 4. As expected, these coefficients are a function of emittances ε_i, being assumed $\varepsilon_{ab}=\varepsilon_2$, $\varepsilon_3=\varepsilon_4=\varepsilon_{TIM}$, and $\varepsilon_5=\varepsilon_6=\varepsilon_{GE}$.

It is important to note here that in the case of the heat transfer through the TIM, a simplification has been made about the process taking place and the corresponding thermal resistance characterizing it.

Underlying the use of this conduction thermal resistance is the assumption that no heat absorption is happening in the inside the TIM. However, as explicitly recognized by the inclusion of the exponent term in Eq. 4, some radiation is absorbed in function of the TIM thickness ($t_4 - t_3$) and the extinction coefficient (μ), which modifies the pure-conduction temperature profile and heat transfer across the component [29]. In order to verify that neglecting the absorbed radiation during the thermal analysis does not affect significantly the results, a more complete model was run, which replaces the thermal resistance by a one-dimensional differential equation taking the absorption effect into account. This model and the corresponding results are not presented in this paper for the sake of brevity, but it can be said that, in general, no divergence of the heat transfer larger than 5% was observed for the parameters analyzed in this work.

2.3. Efficiency

The efficiency (η) for the three types of solar collectors can be expressed as the ratio between the energy reaching the HTF and the incoming solar radiation energy (q_{in}). As implicit defined in Eq. 2, the collection efficiency is expressed as the ratio between the solar radiation reaching the external layer of the GE (q_6) and q_{in}. Therefore, the efficiency of the receiver (η_R) can be defined as the ratio between the collector and the collection efficiencies as follows:

$$\eta_R = \frac{\eta}{\eta_c} = \frac{q_{HTF}/q_{in}}{q_6/q_{in}} = \frac{q_r - q_{loss}}{q_6} \tag{13}$$

Replacing Eqs. 2 through 6 and Eq. 8 into Eq. 13, the general expression for the receiver's efficiency of a solar collector with a TIM yields:

$$\eta = \tau_s \alpha (1 - R_{ra})^2 e^{-\mu(t_4 - t_3)} - \frac{(T_2 - T_7)/R_{tot}}{I_r A_{ab} C \eta_c} \tag{14}$$

In contrast, the efficiency of traditional solar receiver without a TIM can be computed from Eq. 15.

$$\eta_{No\ TIM} = \tau_s \alpha - \frac{(T_2 - T_7)/R_{tot,No\ TIM}}{I_r A_{ab} C \eta_c} \tag{15}$$

where $R_{tot,No\ TIM}$ in Eq. 15 can be calculated from Eq. 11 for FPC and PTC and Eq. 12 for CR.

3. Solar collectors parameters

Dimensional parameters for the three main types of solar collectors studied in this work are presented in Table 5. These parameters were selected based on current operating devices and accepted models available in the literature [2, 23, 57, 58]. For FPC and PTC, the TIM was incorporated between the absorber and the GE. For the external CR, both the TIM and GE were added. The geometrical and physical characteristics of the GE in the CR are adapted from the current features of GEs used in FPCs and/or PTCs. All values presented in Table 5, including the air gaps between the absorber-TIM and TIM-GE, as well as the GE thickness will be maintained constant throughout this work. The only exception is the TIM's thickness, which will be changed to assess its impact in the receiver's performance. Therefore, any change in the TIM's thickness would have the effect of displacing the GE (in FPC and CR) or changing the GE's diameter (in PTC).

The optical parameters and thermal properties for each of the collectors' layers [2, 59-68] are listed in Table 6. The absorber tubes' materials are, commonly, metals due to their high thermal conductivity and mechanical properties. The operating temperatures, and the corrosion resistance at high temperatures are fundamental factors to be considered in the selection of the absorber material. In this work, aluminum for the FPC, B42 copper for the PTC, and 316 stainless steel for the CR are selected. In all cases, the absorber's thermal conductivity is kept constant. Usually, in FPC and PTC, a selective coating is applied onto the absorbers' surface to improve the absorptance in the solar energy spectrum and decrease the emittance in the long-wave spectrum to reduce heat losses [37, 56]. The use of selective coatings allows absorptance (α) values of around 0.95 and emittance (ε_{ab}) values as low as 0.1 [56].

The GE is a thin, transparent, glass cover on the top of FPCs and concentric in PTCs, which provides protection to the absorber and reduces heat losses. For the three types of collectors, a borosilicate glass with a thickness of 3 mm is considered as GE. A constant thermal conductivity (k_{GE}) of 1.25 W/m-k and emittance (ε_{GE}) of 0.85-0.86 are selected. The GE's transmittance (τ_s) is a material property that specifies the fraction of the solar radiation passing through the glass. Transmittance values as high as 0.97 are possible using anti-reflective coatings [66]. In this work, a constant value of τ_s = 0.92 is considered. As previously mentioned, the use of TIMs in the three types of collectors is the strategy analyzed in this work to enhance the receiver's performance due to a reduction of radiative and

convective heat losses. The TIM's extinction coefficient (μ) is an indicator of the amount of radiation absorbed by this material at a specific wavelength. μ usually varies from ~ 4 m^{-1} in good quality glass to ~ 30 m^{-1} for typical window glass containing iron [56, 69]. For solar applications, high quality glasses may have extinction coefficients as low as ~ 1 m^{-1} [28], which is the reference value taken in this work. In addition to the absorption effect, around 4% of the solar radiation is reflected in each of the TIM's surfaces (outer and inner). Note that the reference TIM's optical and thermal properties (k_{TIM}, μ, ε_{TIM}, ε_{ra}), presented in Table 6, are the same for the three collectors. This set of parameters will be changed in the corresponding sections indicated in Table 6 in order to study the effect of each of these variables in the solar receiver's performance.

Table 5. Dimensional parameters for FPCs, PTCs, and CR collectors.

Parameter	Value
Flat plate collector	
Width, H (m) [2]	1.0
Length, L (m) [2]	2.0
Absorber channel thickness, t_1 (m) [2]	0.02
Absorber wall thickness, $t_2 - t_1$ (mm)	2
Absorber area, A_{ab} (m^2)	2
Air gap, $t_3 - t_2$ (mm)	10
TIM's thickness, $t_4 - t_3$ (mm), (Subsec. 4.1)	20
Air gap, $t_5 - t_4$ (mm)	10
GE's thickness, $t_6 - t_5$ (mm)	3
Parabolic trough collector	
Receiver length, L (m) [57]	4
Absorber outer diameter, $2t_2$ (m) [57]	0.07
Tube wall thickness, $t_2 - t_1$ (mm) [57]	2
Projected area of absorber, A_{ab} (m^2)	0.28
Air gap, $t_3 - t_2$ (mm)	10
TIM's thickness, $t_4 - t_3$ (mm), (Subsec. 4.2)	20
Air gap, $t_5 - t_4$ (mm)	10
GE's thickness, $t_6 - t_5$ (mm) [57]	3
Central receiver	
Receiver height, H (m) [23]	10.5
Receiver diameter, D (m) [23]	8.5
Absorber tubes outer diameter, $2t_2$ (m) [58]	0.0603
Tube wall thickness, $t_2 - t_1$ (mm) [58]	1.65
Projected irradiated area of each absorber, A_{ab} (m^2)	0.63
Air gap, $t_3 - t_2$ (mm)	10
TIM's thickness, $t_4 - t_3$ (mm), (Subsec. 4.3)	20
Air gap, $t_5 - t_4$ (mm)	10
GE's thickness, $t_6 - t_5$ (mm)	3

Table 6. Optical parameters and thermal properties for FPCs, PTCs, and CR collectors.

Parameter	Flat plate	Parabolic Trough	Central receiver
Absorber			
Material	Aluminum	B42 Copper	316 Stainless steel
α	0.95 [2]	0.95	0.95 [59]
k_{ab} (W/m-K)	190 [60]	400 [61]	23.8 [62]
ε_{ab}	0.1 [63]	0.27 [57]	0.85 [64]
Support bracket			
Material	Crystal wool	304 Stainless steel	316 Stainless steel
k_{dis} (W/m-K)	0.038 [2]	16[62]	23.8 [62]
A_{dis} (m^2)	2	0.01	0.0003
L_{dis} (m)	0.05	1	4.2
TIM			
k_{TIM} (W/m-K)	1.0 (0.1 – 5.0, Sec. 4.1)	1.0 (0.1 – 5.0, Sec. 4.2)	1.0 (0.1 – 5.0, Sec. 4.3)
μ (m^{-1})	1 (1 – 8, Sec. 4.1)	1 (1 – 8, Sec. 4.2)	1 (1 – 8, Sec. 4.3)
ε_{TIM}	0.20 (0.05 – 0.95, Sec. 4.1)	0.20 (0.05 – 0.95, Sec. 4.2)	0.20 (0.05 – 0.95, Sec. 4.3)
R_{ra} (%)	4 [28]	4	4
GE			
k_{GE} (W/m-K)	1.25	1.25 [65]	1.25
τ_s	0.92 [2]	0.92 [66]	0.92
ε_{GE}	0.87 [4]	0.86 [57]	0.87
Air gaps and environment			
h_{3-4} (W/m^2-K)	5	5	5
h_{5-6} (W/m^2-K)	5	5	5
h_7 (W/m^2-K)	20 [67]	20 [67]	20 [67]
Collection system			
C	1	30 (15 – 100, Sec. 4.4)	400 (100 – 1500, Sec. 4.4)
η_c	1	0.8 [57]	0.6 [68]

A fraction of thermal losses occurs along the support brackets. Values for the bracket's cross-sectional area (A_{dis}), length (L_{dis}), and thermal conductivity (k_{dis}), for each type of collector, are presented in Table 6. In the case of the PTC, these supports are attached to the absorber tubes at the collector's focal line, providing structural support. For a CR, the brackets support the absorber tubes, fastening them to the central structure in the receiver. The values of A_{dis} and L_{dis} for PTCs and CR collectors are estimated based on their receiver's geometries, and are comparable with the values reported for similar systems [17, 57, 58]. The bracket's thermal conductivity for the PTCs is $k_{dis} = 16$ W/m-K, which corresponds to a 304 stainless steel material, commonly used in outdoors structures [62] and PTC absorbers [57]. For the CR at thermal conductivity value of k_{dis} = 23.8 W/m-k [62] is used, which is assumed to be equal to k_{ab}. In the case of FPC, the system is supported by the bottom insulation layer, which, in this particular case, is composed of crystal wool. This material has a low thermal conductivity of $k_{dis} = 0.038$ W/m-K [2], an area of A_{dis} =2 m^2, and a thickness of $L_{dis} = 0.05$ m. Note that these values agree with dimensions of real FPCs [2, 70].

Regarding the collection system, the collection efficiency (η_c) is a factor applied to PTCs and CRs. This efficiency accounts for energy losses due to tracking errors, shadows, mirror alignment, dirt on the mirrors, etc. For PTCs, η_c has been estimated as ~ 0.8 [57], while an annual collection efficiency of about 0.6 has been estimated for CRs [68]. In concentrating solar devices, the concentration ratio (C) is a factor that quantifies the increment in the direct-normal solar radiation flux reaching the absorber's surface after it is reflected and redirected to a focus point or line. C values usually vary between 15 and 45 in PTCs, and 100 and 1500 in CRs [4]. The reference value of the concentration ratio and the analyzed range of this parameter are indicated in Table 6. Finally, in order to simplify the analysis, the convection heat transfer coefficients have been considered constant in this work. The values of h_{3-4}, h_{5-6}, and h_7 are commonly used in the literature [67] and are also listed in Table 6.

4. Results and Analysis

The effect of integrating a TIM into each of the three types of solar collectors (FPC, PTC and CR) is assessed in this section. Different TIM's properties including the emittance, thermal conductivity, extinction coefficient, and thickness are studied and evaluated in terms of solar the collector's efficiency and thermal losses. Performances of solar collectors with different TIM's properties are analyzed and compared with the respective conventional configurations without a TIM.

4.1. Flat plate collector

The efficiency and thermal losses of a traditional type and TIM-incorporated flat plate collectors, as a function of the inner absorber's surface temperature (T_{ab}), are presented in Figs. 3 to 6. As indicated before, the values for the parameters used are listed in Tables 5 and 6. It is well know that higher working fluid temperatures favor power cycles efficiencies. However, they can also increase thermal losses to the environment in solar collectors. Note that a high T_{ab} is a relative condition that depends on the collector technology in question. It, typically, represents the upper temperatures range where a specific type of collector usually operates. From Figs. 3 to 6, the reduction in efficiency with T_{ab} can be lessened with the incorporation of transparent insulation materials. These figures not only show the advantages of using a TIM but also the effect of TIM's thermal and optical properties on the collectors' efficiency and thermal losses.

The performance of FPC with different TIM's emittances is shown in Fig. 3. For the values of parameters used and low absorber temperatures ($T_{ab} < 50$), efficiencies between 69% and 82% can be achieved in a traditional collector. A better performance of the system is possible, for larger T_{ab}, by integrating a TIM into the traditional collector configuration, see Fig. 3a. Several scenarios with different TIM's emittance values are displayed in this figure. Lower ε_{TIM} values are desired to achieve higher efficiencies due to a reduction in the TIM's outer surface temperature, and consequently a reduction in heat losses, see Fig 3b. The use of a TIM leads to a better performance of the system after 51°C for ε_{TIM} = 0.05 and 71°C for ε_{TIM} = 0.95. For instance, a high absorber temperature of 120°C results in an efficiency of ~ 34% for a traditional FPC, which is improved to ~ 41% and ~ 51% for a TIM with ε_{TIM} = 0.95 and ε_{TIM} = 0.05 is, respectively, introduced. The corresponding thermal losses are reduced from about 1 kW in the traditional configuration to 0.74 kW for ε_{TIM} = 0.95 and 0.56 kW for ε_{TIM} = 0.05, when $T_{ab} = 120$°C.

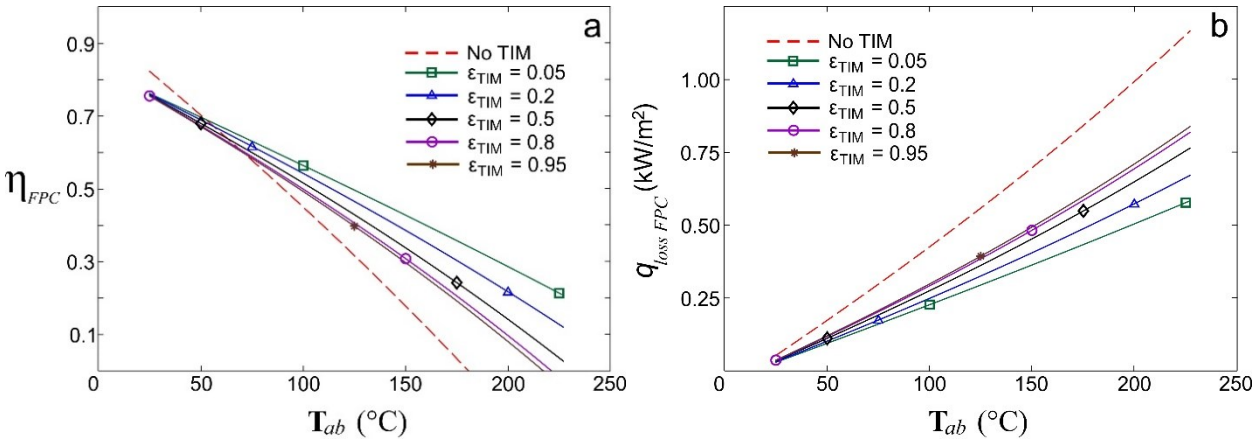

Figure 3. Effect of TIM's emittance (ε_{TIM}) on a) efficiency and b) thermal losses for flat plate collectors.

The effect of TIM's thermal conductivity on the efficiency and thermal losses of a FPC is presented in Fig. 4. Lower thermal conductivities imply a better thermal insulation effect through the TIM and consequently a reduction in the heat losses. According to Fig 4a, the FPC performance is enhanced for absorber temperatures greater than 43°C if k_{TIM} = 0.1 W/m-K and 59°C if k_{TIM} = 5.0 W/m-K when a TIM is incorporated. A considerable improvement in the efficiency and reduction of heat losses are achieved for lower k_{TIM} values, i.e. $k_{TIM} \leq 0.1$ W/m-K. Less significant changes in η_{FPC} and $q_{loss\,FPC}$ are observed for thermal conductivities between 0.5 W/m-K to 5.0 W/m-K. From these results, it is clear that the system is more sensitive at low k_{TIM} values. Then the quest for a superior performance must include a TIM with very low thermal conductivities, taking into account that having a TIM with k_{TIM} =

0.5 W/m-K does not represent a significant improvement when compared with values ten times higher. Considering a traditional FPC, which maximum operating temperature limit is around 120°C [2], the efficiency can be enhanced from ~ 34% to ~ 46% for k_{TIM} = 5.0 W/m-K and to ~ 57% for k_{TIM} = 0.1 W/m-K. The thermal losses, in turn, are diminished from ~ 1 kW in the traditional FPC to 0.65 kW for k_{TIM} = 5.0 W/m-K and 0.45 kW for k_{TIM} = 0.5 W/m-K. Note that these values are calculated with a reference emittance of ε = 0.2 (see Table 6). It is expected that the combination of a lower thermal conductivity and a lower thermal emittances ($\varepsilon < 0.2$) lead to additional improvements in efficiency and reduction in heat losses.

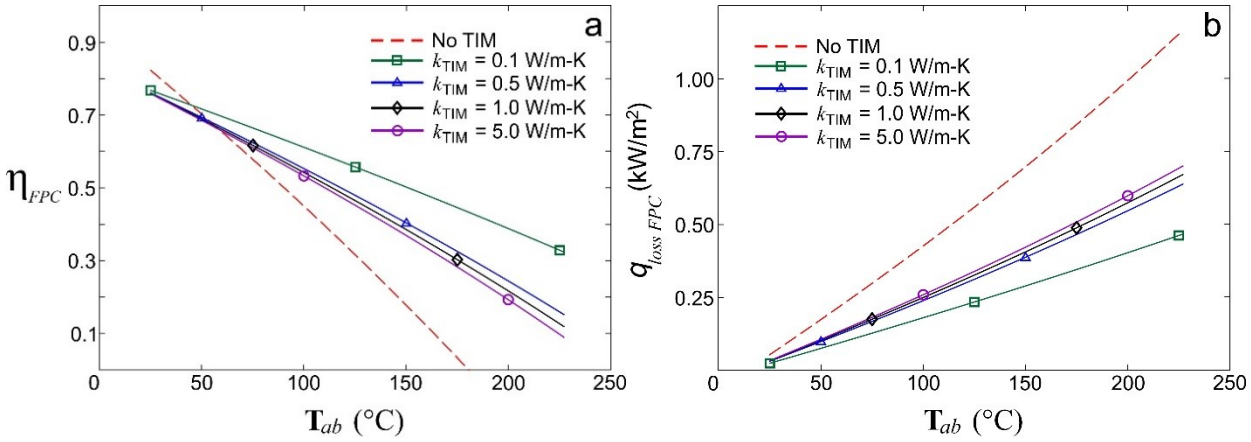

Figure 4. Effect of TIM's thermal conductivity (k_{TIM}) on a) efficiency and b) thermal losses for flat plate collectors.

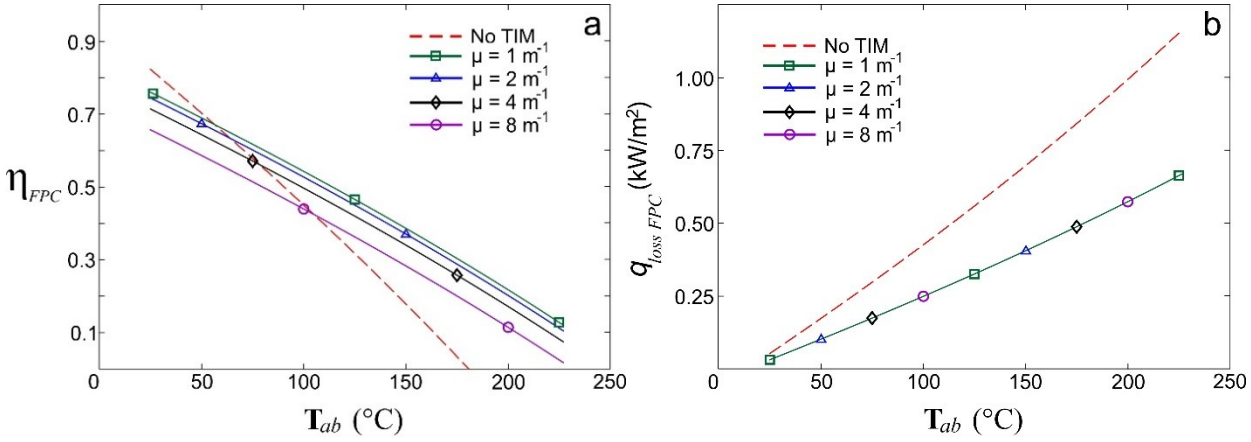

Figure 5. Effect of TIM's extinction coefficient (μ) on a) efficiency and b) thermal losses for flat plate collectors.

Another important TIM's property is the extinction coefficient. The effect of this parameter on the efficiency and thermal losses of a FPC is presented in Fig. 5. Lower μ values imply a lower absorption of the incoming solar radiation or a more transparent material, which results in an increased efficiency

due to a greater energy input. Changes in μ, do not affect the efficiency reduction rate as a function of T_{ab} (the slope of the efficiency profiles remain constant), see Fig 5a. This means that the thermal losses, in a TIM-incorporated collector, are independent of the extinction coefficient as observed in Fig. 5b. This behavior have two implications: first, changes on the efficiency of the collector as a function of μ are not caused by a reduction in thermal losses but a change in the input of solar irradiation, unlike what happens in the case of other TIM's properties such as k_{TIM} and ε_{TIM}. Second, changes in the slope of efficiency curves are caused by variations in the heat losses, which in turn can be modified with some TIM's properties as shown in Figs. 3b and 4b. For μ = 8 m^{-1}, the collector with a TIM is more efficient, than the conventional one, at $T_{ab} >$ ~ 103°C. The T_{ab} from which the efficiency of a TIM-incorporated collector surpasses the efficiency of a traditional one, can be reduced up to ~ 55°C for μ = 1 m^{-1}. This means that lower the TIM's extinction coefficients, larger the expansion of the absorber temperature domain, where a collector with a TIM operates more efficiently than a traditional one.

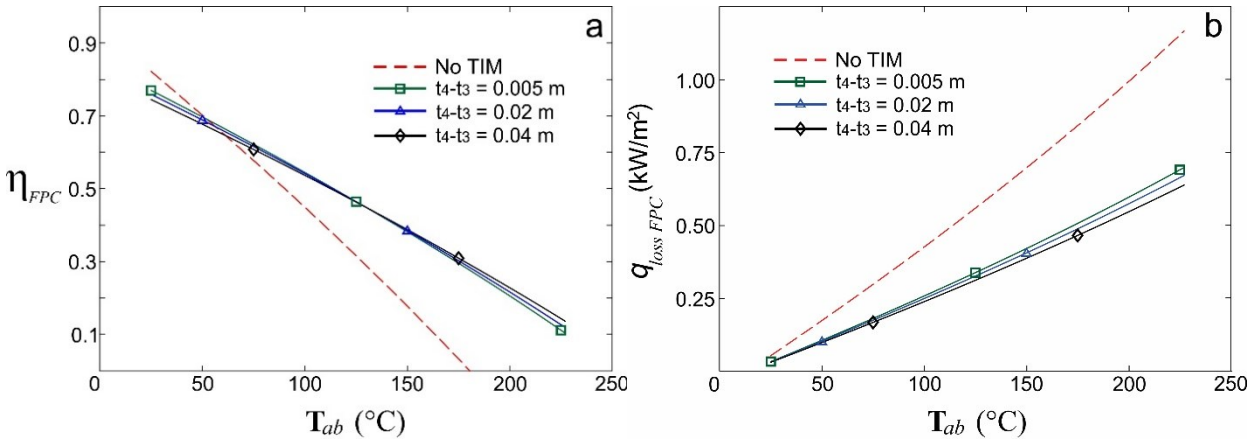

Figure 6. Effect of TIM's thickness ($t_4 - t_3$) on a) efficiency and b) thermal losses for flat plate collectors.

The effect of the TIM's thickness on the efficiency and thermal losses of a FPC, as a function of the T_{ab}, is presented in Fig. 6. Only a small influence of this parameter on the collector's performance is observed. A greater thickness slightly reduces the energy input at low temperatures ($T_{ab} \lesssim$ 100°C), with the efficiency of the collector undergoing a short reduction. At high temperatures ($T_{ab} \gtrsim$ 150°C), thicker thicknesses imply a more significant insulation effect that translates in some reduction of thermal losses, see Fig. 6b. At $T_{ab} \gtrsim$ 150°C, the TIM thickness starts to exert a stronger influence in the heat loss reduction that overcomes the reduction on the solar radiation, with higher efficiencies on the FPC being achieved. A balance between these two competitive effects, around 127°C $\lesssim T_{ab} \lesssim$ 132°C, results in a similar efficiency for the analyzed thickness values.

4.2. Parabolic trough collector

The results from the analysis of integrating a TIM into parabolic trough collectors, as a function of the T_{ab}, are presented in Figs. 7 to 10. It can be observed in these figures that higher efficiencies and lower heat losses are possible in TIM-incorporated collectors operating at relatively high temperatures, when compared with a traditional PTC. A strong influence of TIM's parameters on the collector's performance is also evident. The effect of TIM's emittance on the efficiency and thermal losses of this type of collector is displayed in Fig. 7. Lower ε_{TIM} values reduce the efficiency decay rate as a function of T_{ab}, maintaining relatively high the collector's efficiencies at high temperatures, with respect to the reference collector without a TIM. A larger benefit can be accounted for ε_{TIM} = 0.05 that allows a superior efficiency for $T_{ab} >$ 176°C, reaching about 59% at $T_{ab} =$ 400°C. At this temperature, a traditional PTC works with an efficiency of less than 30%, see Fig. 7a. High emittance values, for instance ε_{TIM} = 0.95, can also provide some improvement in the receiver's performance for T_{ab} greater than 287°C, allowing an efficiency of 36% at $T_{ab} =$ 400°C. Increments in η_{PTC}, as a result of low emittances, are driven by a reduction in the heat losses as can be observed in Fig. 7b. At $T_{ab} =$ 400°C, the thermal losses of a traditional PTC are about 3.9 kW. With the integration of the TIM, these losses are lowered to ~ 2.9 kW and 1.3 kW for ε_{TIM} = 0.95 and ε_{TIM} = 0.05, respectively.

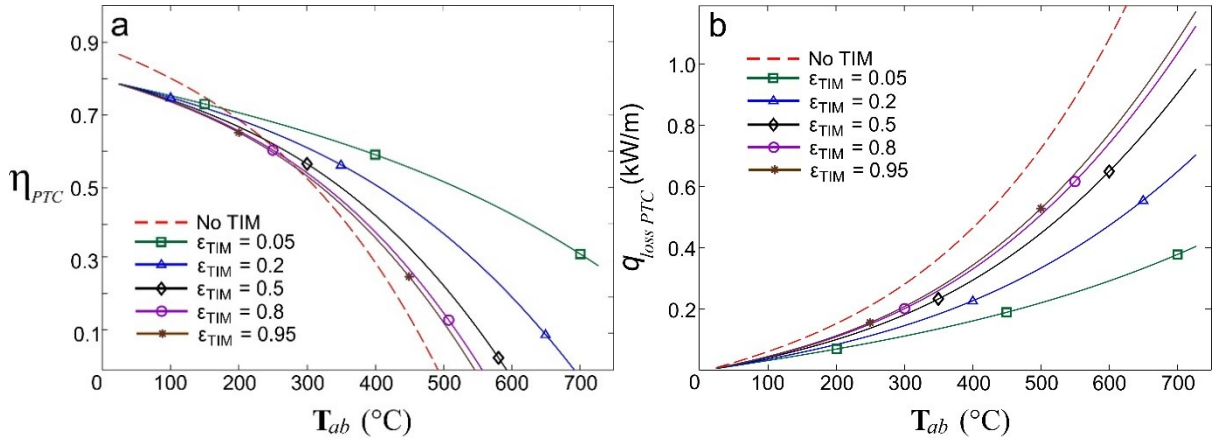

Figure 7. Effect of TIM's emittance (ε_{TIM}) on a) efficiency and b) thermal losses for parabolic trough collectors.

The traditional parabolic through collector presents the highest efficiency at low T_{ab}, however it reduces dramatically with the increment in the temperature due to a substantial growth in heat losses. These losses can be minimized by incorporating a TIM with low thermal emittance, as analyzed previously, and low thermal conductivity as can be seen in Fig. 8. Small k_{TIM} values do not affect the

incoming radiation but exert an insulating effect to the energy losses that allow higher efficiencies at high absorber temperatures. Likewise of what happens in FPC, low values of TIM's thermal conductivity ($k_{TIM} < 0.1$ W/m-K) have a stronger impact on the efficiency. The efficiency of a TIM-incorporated PTC surpasses the traditional one at T_{ab} = 162°C for k_{TIM} = 0.1 W/m-K, and T_{ab} = 207°C for k_{TIM} = 5.0 W/m-K. A considerable high efficiency of ~ 61% is still achieved in the TIM-incorporated collector with k_{TIM} = 0.1 W/m-K and operating at T_{ab} = 400°C. It also increases, in a lower scale, to ~ 49% for k_{TIM} = 5.0 W/m-K and ~ 52% for k_{TIM} = 0.5 W/m-K for the same temperature, see Fig. 8a. The corresponding thermal losses are diminished to 1.2 kW in a TIM-incorporated collector with k_{TIM} = 0.1 W/m-K. Also reductions in thermal losses of between 1.8 kW and 2.0 kW for k_{TIM} = 0.5 kW/m-K and k_{TIM} = 5.0 kW/m-K are achieved, respectively, see Fig. 8b.

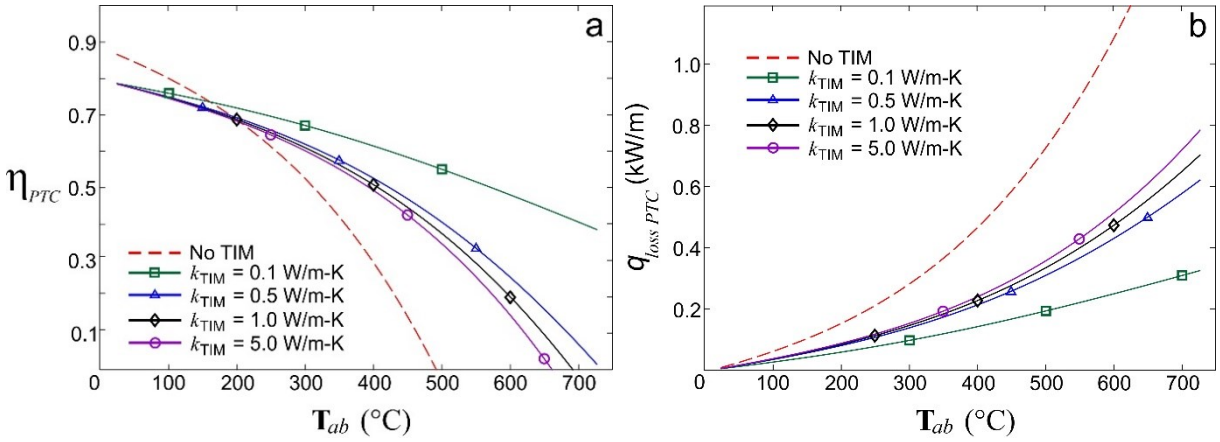

Figure 8. Effect of TIM's thermal conductivity (k_{TIM}) on a) efficiency and b) thermal losses for parabolic trough collectors.

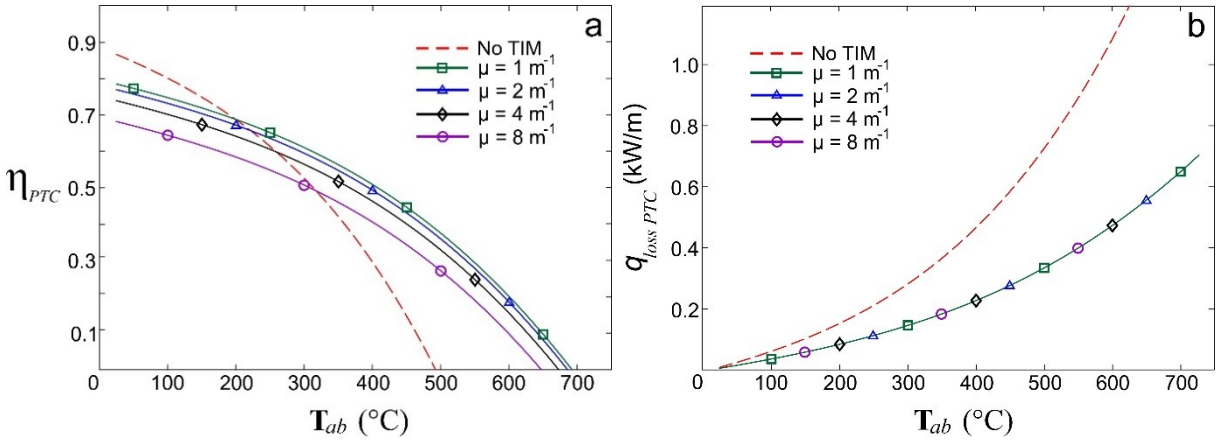

Figure 9. Effect of TIM's extinction coefficient (μ) on a) efficiency and b) thermal losses for parabolic trough collectors.

The effect of TIM's extinction coefficient on the efficiency and heat losses of parabolic though collectors with and without a TIM are presented in Figs. 9a and 9b, respectively. In general, $\mu < 8$ m^{-1} is beneficial to maintain higher efficiencies for $T_{ab} > 319$°C. The efficiency profiles values for a PTC including a TIM are shifted downwards with the increment in the extinction coefficient, which implies a larger amount of solar energy absorbed along the TIM thickness. As previously mentioned in the analysis of a FPC, the thermal losses are reduced in a TIM-incorporated PTC; however, they are independent of μ as can be seen in Fig. 9b. Again, the efficiency improvements achieved with lower μ values are driven by a more transparent TIM that exerts a smaller resistance to the solar radiation flux.

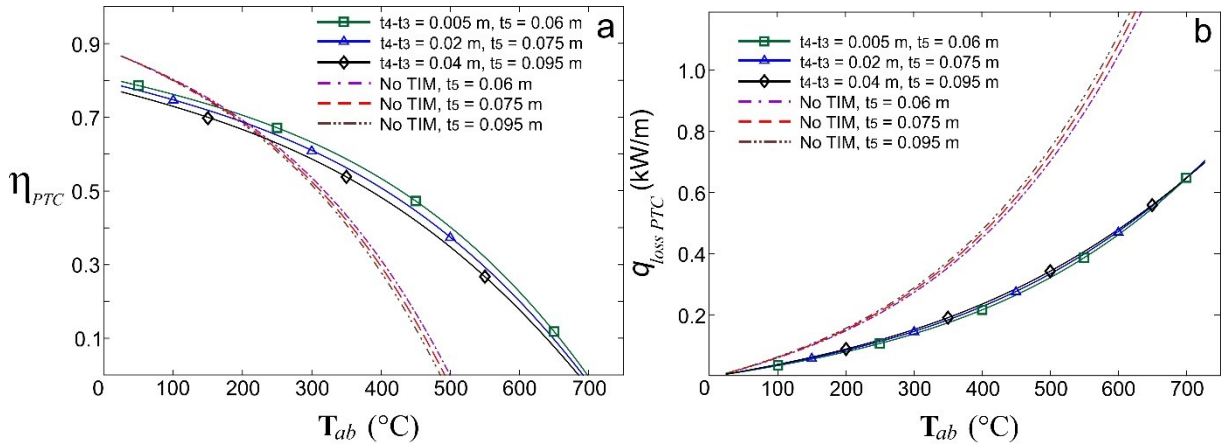

Figure 10. Effect of TIM's thickness ($t_4 - t_3$) on a) efficiency and b) thermal losses for parabolic trough collectors.

The TIM thickness also influences the efficiency and thermal losses of a PTC. Figures 10a and 10b present the behavior of PTC with a TIM with thicknesses of 5 mm, 20 mm and 40 mm. The conventional PTC achieves higher efficiencies at low absorber temperatures ($T_{ab} \lesssim 179$°C). For T_{ab} greater than ~ 201°C, TIM-incorporated PTCs accomplish a superior performance. Thicker TIMs slightly reduce the solar energy input and therefore the PTC's efficiency, see Fig. 10a. Comparing with other properties such as ε_{TIM}, k_{TIM} and μ, less improvement in the efficiency can be achieved with TIM's thickness ranging between 5 mm and 40 mm. For instance, a traditional PTC can operate at an efficiency of about 29% at T_{ab} = 400°C. At this temperature, the integration of a TIM into the PTCs increases η_{PTC} to 48% for $t_4 - t_3 < 40$ mm, but only five additional percentage points can be obtained for $t_4 - t_3 < 5$ mm. It can be noticed that any change in the thickness also changes the diameter of the GE, so the air gaps remain constant independent of the TIM's thickness. These geometric modifications, in GE's diameter of PTCs, when the TIM's thickness is augmented or diminished imply a change in the surface

area of the GE, which slightly impact the thermal losses of the traditional collector's efficiency, and also affect its efficiency. This effect does not occur in FPC and CR because, in these cases the GE's surfaces are flat, and any change in the TIM thickness is only reflected in a displacement of this layer which surface remains constant. The behavior of thermal losses as a function of the TIM's thickness is, relatively different of what was observed in FPCs. From Fig. 10b, losses are practically independent of the TIM's thickness. Only a small variation in heat losses profiles of TIM-incorporated PTCs can be observed for intermediate absorber temperatures (250°C $< T_{ab} <$ 650°C), which are expected to exert a minor impact in the receiver's efficiency.

4.3. Central receiver

The efficiency and thermal losses of a traditional and a TIM-incorporated external central receiver, as a function of the T_{ab}, are presented in Figs. 11 to 14. In general, two different scenarios can be identified: low absorber temperatures where a traditional receiver exhibits a higher efficiency when compared with the receiver with a TIM and GE, and high absorber temperatures where this last receiver still operates efficiently, while the traditional one is every time less efficient, as the temperature rises, due to an accelerated increment in thermal losses, see Figs. 11b, 12b, 13b and 14b. The addition of a TIM and GE reduce the thermal losses but also the solar radiation reaching the absorber. This is why the new design initially presents a lower efficiency, but the reduction of heat losses attributed to the presence of the TIM and GE leads to an efficient operation at high temperatures.

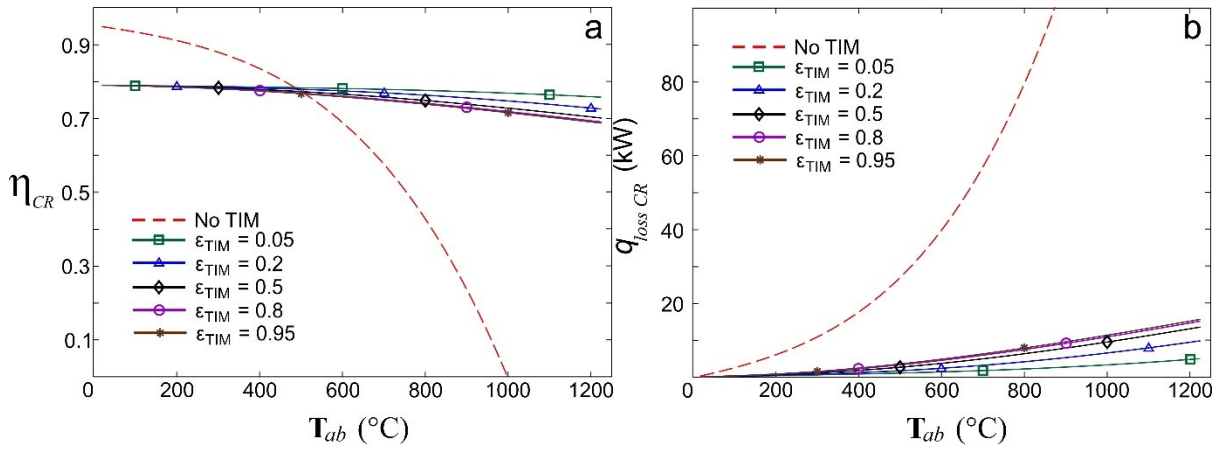

Figure 11. Effect of the TIM's emittance (ε_{TIM}) on a) efficiency and b) thermal losses for external central receivers.

In Figs. 11 to 14, the effects of the TIM's emittance, thermal conductivity, extinction coefficient and thickness on the receiver's performance are presented and compared with a traditional CR. As it

was observed in the FPC and PTC, low emittance values reduce heat losses allowing higher efficiencies at high absorber temperatures. For $T_{ab} < 484$°C, the efficiency of a traditional receiver is the highest starting at a value of ~ 95% at T_{ab} ~ 20°C, and decreasing to ~ 78% at T_{ab} = 484°C. In this temperature range, a receiver with a TIM and GE exhibits an initial efficiency of about 79% which reduces in approximately one to two percentage points for the analyzed ε_{TIM} values, see Fig. 11a. The thermal emittance does not have a strong influence at T_{ab} below 484°C. Lower ε_{TIM} results in higher efficiencies; however, this effect is more significant as the absorber temperatures increases. Emittances as low as 0.05 imply an efficiency of the solar collector of about 77% at T_{ab} = 800°C, while only an efficiency of around 42% are possible for the reference traditional one at this temperature. Low emittances improve the receiver's performance due to a considerable reduction in heat losses as can be observed in Fig. 11b.

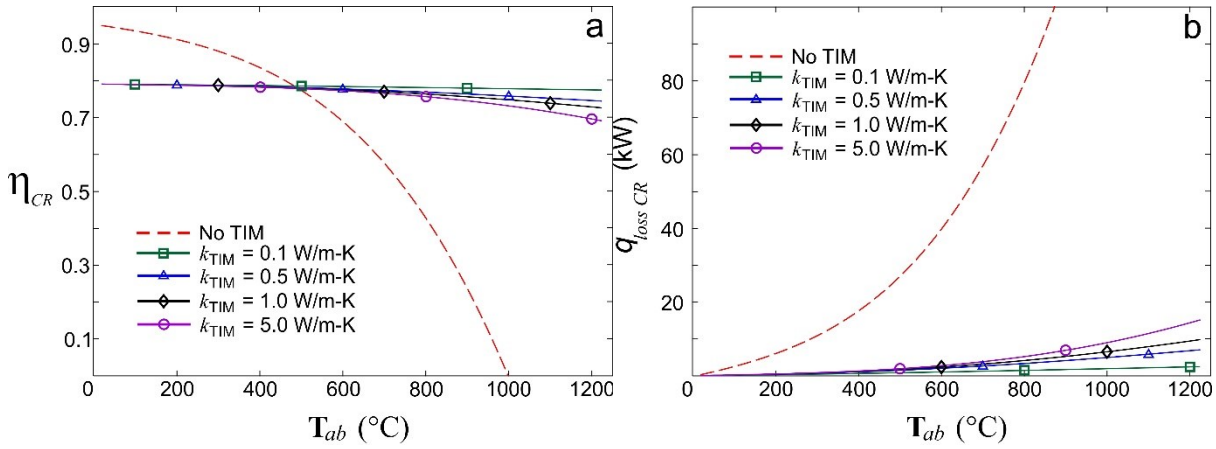

Figure 12. Effect of the TIM's thermal conductivity (k_{TIM}) on a) efficiency and b) thermal losses of external central receivers.

The influence of the TIM's thermal conductivity on the collector's performance and heat losses are displayed in Fig. 12. The effect of this property on the efficiency is similar to the effect of ε_{TIM}. For $T_{ab} < 484$°C, the efficiency of the TIM and GE-incorporated receiver is practically identical for the studied k_{TIM} values. Lower TIM's thermal conductivities favor the efficiency; however the effect of this property becomes stronger at high temperatures. Note that a solar receiver having a TIM with a low thermal conductivity of k_{TIM} = 0.1 W/m-K maintains the efficiency almost constant, see Fig. 12a. Only a reduction in η_{CR} from ~ 79% to ~ 77% occurs in the entire T_{ab} range (~ 20°C to ~ 1223°C), which is caused by the insulating effect that reduces heat losses, see Fig. 12b.

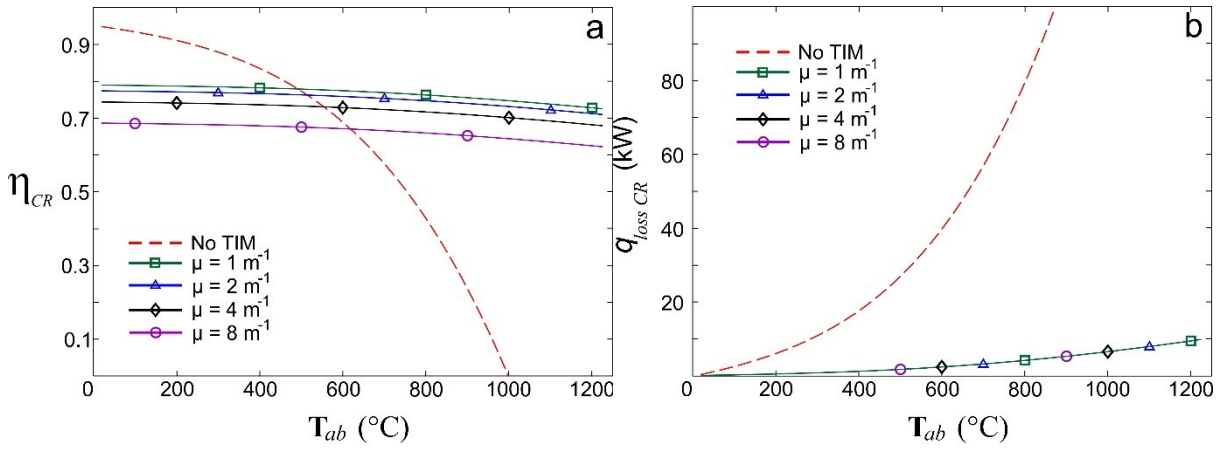

Figure 13. Effect of the TIM's extinction coefficient (μ) on a) efficiency and b) thermal losses for external central receivers.

Figure 13 shows the influence of the TIM's extinction coefficient on the efficiency and heat losses of a central receiver. These results are presented as a function of T_{ab} and are compared with the efficiency and thermal losses of a traditional CR configuration. Lower μ values imply more transparent TIMs. In other words, the TIM allows more solar radiation to cross as the extinction coefficient becomes smaller. Then, the efficiency of the solar collector increases when μ is reduced. At difference of ε_{TIM} and k_{TIM}, a reduction in the extinction coefficient, implies a substantial increment in the efficiency at the entire absorber temperature range, see Fig. 13a, and not only at high temperatures. Larger μ means more radiation absorption, and thus a reduction in the efficiency caused by a lower solar energy reaching the absorber. The efficiency decay rate can be controlled by changing the emittance and thermal conductivity (slope of η_{CR}- T_{ab} curve), while μ determines the initial CR's efficiency and how much one of the η_{CR} profiles parallel displaces with respect to the other. The integration of a TIM into the CR substantially reduces thermal losses; but they are independent on μ as can be observed in Fig. 13 b. This means that the extinction coefficient does not exert any influence on the energy going out of the receiver and the insulation effect is mainly attributed to ε_{TIM} and k_{TIM}.

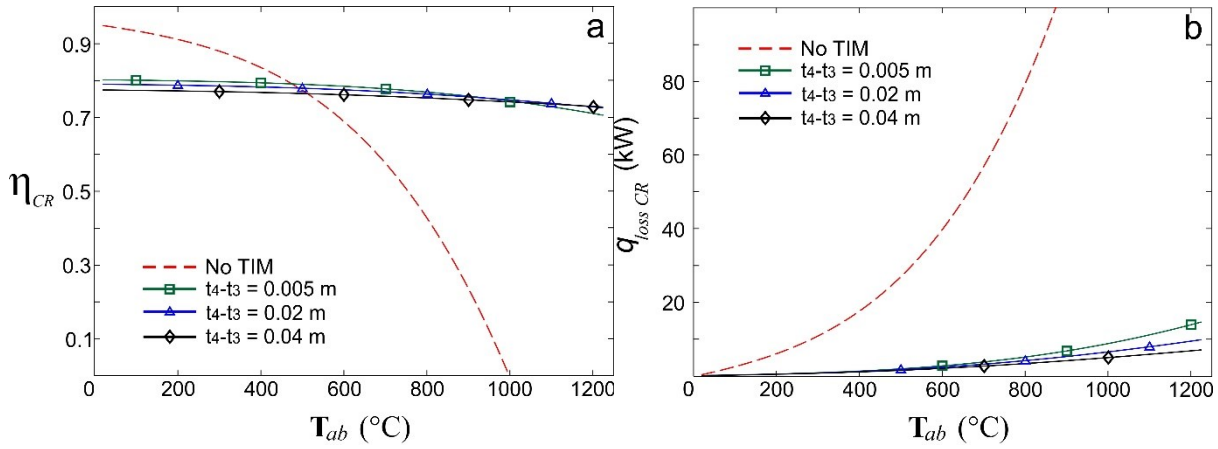

Figure 14. Effect of the TIM's thickness ($t_4 - t_3$) on a) efficiency and b) thermal losses for external central receivers.

The effect of the TIM's thickness on the performance of a central receiver, as a function of T_{ab}, is displayed in Fig. 14. The thickness affects both, the solar radiation entering the receiver (see Eqs. 4 and 5) and the energy losses (see thermal resistance $R_{cd,2}$ in Table 1). At low temperatures ($T_{ab} <$ ~ 400°C), thicker TIMs represent a slight reduction in the solar radiation (Eqs. 4 and 5) and consequently a small reduction in η_{CR}. The thermal losses, instead, are not significantly affected at these temperatures. Then, the efficiency profiles are almost parallel one to each other, while the thermal losses profiles coincide. For $T_{ab} >$ ~ 600°C, the thickness starts to cause an insulating effect which is evidenced in lower heat losses when $t_4 - t_3$ = 40 mm, as can be seen in Fig. 14b. A reduction in these losses, allows the receiver with a thicker TIM ($t_4 - t_3$ = 40 mm) to maintain larger efficiencies that even surpasses the efficiency of thinner-TIM receivers after ~ 1000°C. In this particular case, a TIM thickness of 40 mm is more convenient for T_{ab} over 1000°C, thinner TIMs ($t_4 - t_3$ = 20 mm and $t_4 - t_3$ = 5 mm) are more appropriated in the range ~ 512°C $< T_{ab} <$ ~ 1000°C, while a traditional central receiver should be operated at $T_{ab} <$ ~ 476°C for the selected concentration ratio and design conditions.

4.4. General comparison

Figure 15 presents the efficiency profiles for FPCs, PTCs, and CRs for different TIM's properties. The reference condition (TIM ref) corresponds to the TIM's properties listed in Table 6. The other two conditions, TIM 1 and TIM 2 are defined in terms of TIM's properties as follows: TIM 1: ε_{TIM} = 0.9, k_{TIM} = 1.0 W/m-K, μ = 4 m^{-1}, t_4 - t_3 = 0.02 m. TIM 2: ε_{TIM} = 0.1, k_{TIM} = 0.5 W/m-K, μ = 1 m^{-1}, t_4 - t_3 = 0.02 m. The efficiency profiles of solar receivers with different TIMs are compared with the respective traditional configuration. The operating ranges according to the collection technology are clearly differentiated. It

can be observed that in all cases the solar receivers with the TIM exhibit superior performance at high T_{ab}. Even for TIM 1, which properties are quite modest, the efficiency is improved at higher temperatures. The properties of TIM 2, in turn, are selected to exemplify the behavior of the receiver with a TIM with a high quality that can be implemented in any of the three solar collectors to obtain a superior performance. Finally, there is a wide range of semitransparent materials that can be used as TIMs. The proper selection of TIM's properties, to achieve a high performance, depends on T_{ab}. In general, an appropriated TIM must be characterized by a low emittance, low thermal conductivity, high transmittance and low extinction coefficient.

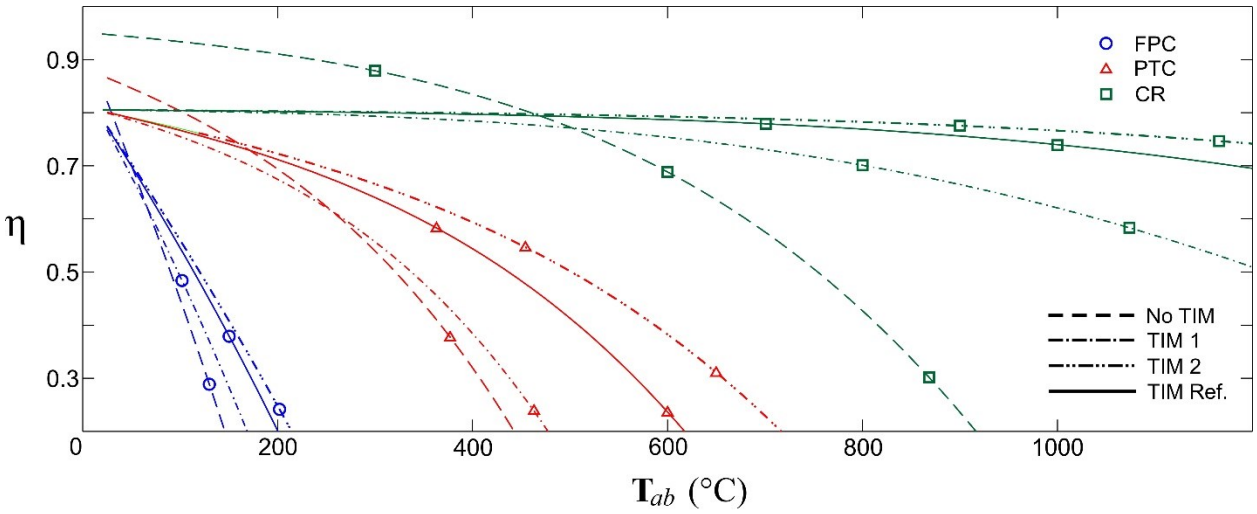

Figure 15. Efficiency of FPC, PTC and CR collectors without a TIM and with two different TIM's properties. TIM 1: ε_{TIM} = 0.9, k_{TIM} = 1.0 W/m-K, μ = 4 m^{-1}, t_4 - t_3 = 0.02 m. TIM 2: ε_{TIM} = 0.1, k_{TIM} = 0.5 W/m-K, μ = 1 m^{-1}, t_4 - t_3 = 0.02 m.

5. Concentration ratio

The concentration solar ratio (C) is another important characteristic in solar-based power generation cycles. The direct-normal solar radiation is reflected in a heliostat, dish or parabolic mirrors and then it is concentrated in a focal line or point to run a power generation cycle. In general, larger C values involve higher plant capacities. It also results in larger investments and operating costs due to bigger number of reflectors, more robust components and resistant materials to operate at high temperatures. The concentration ratio also depends on the CSP technology. PTC usually operates at concentration ratios between 15 and 45, while C values ranging between 100 and 1500 are typical used

in central receiver configurations [4]. In general, greater concentration ratios allow higher operating temperatures and consequently higher cycle efficiencies. In Fig. 16, the efficiency profiles as a function of the T_{ab} of PTC collectors are presented for three different values of C. The efficiency of both, the traditional and TIM-incorporated PTCs, rises with C. Increments in the concentration ratio also displaces the limit absorber temperature ($T_{ab\ lim}$) to higher values. In this work, $T_{ab\ lim}$ corresponds to the temperature from which the efficiency of the new design (collector with a TIM) surpasses the efficiency of a conventional solar receiver. Then, larger $T_{ab\ lim}$ means greater ranges of absorber temperatures where the performance of traditional PTCs is superior. According to the profiles displayed in Fig. 16, the TIM-incorporated PTC becomes more efficient at $T_{ab} > 153$°C, $T_{ab} > 239$°C, and $T_{ab} > 301$°C for concentration ratios of 20, 40 and 60, respectively.

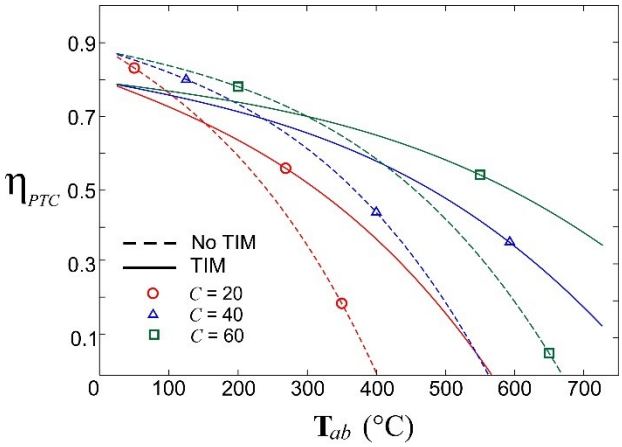

Figure 16. Effect of the concentration ratio on the performance for parabolic trough collectors.

Figures 17a and 17b, present efficiency contours of TIM-incorporated PTCs (Fig. 17a) and traditional PTCs (Fig. 17b) as a function of C and T_{ab}. In both figures, the limit T_{ab} is displayed as a solid line. Comparing both contours, it is clear that higher η_{PTC} are obtained in the upper region above the $T_{ab\ lim}$ line for TIM-incorporated PTCs. The lower region, conversely, corresponds to the concentration ratio and T_{ab} where the traditional PTC is more efficient. Particularly, a $T_{ab\ lim}$ of approximately 390°C is obtained for a relatively high concentration ratio (in PTCs) equal to 100, with a corresponding efficiency of ~ 71%. The efficiency can be maintained high at high absorber temperatures ($T_{ab} > 390$°C) if a TIM is integrated into the PTC. From the contours, it is clear that the use of an additional layer, in this case the TIM, reduces the solar radiation reaching the absorber. This effect has a strong impact in the efficiency at low temperatures. However, the TIM also produces an insulation effect that reduces the thermal losses and becomes stronger at high T_{ab} as can be observed in Fig. 17c. The important outcome from

this analysis is that the efficiency, of a TIM-incorporated receiver operating at low temperatures, is not strongly impacted, and values of more than 70% can still be reached, while a traditional PTC operating at high temperatures, or after $T_{ab\ lim}$, could reduce its efficiency considerably. This aspect is further important considering that higher operating temperatures are desired to obtain high conversion cycles efficiencies. From Fig. 17c, the integration of the TIM reduces the thermal losses in the range $15 \leq C \leq 100$. This effect is stronger at large concentration ratios because greater energy inputs result in higher temperatures and therefore larger heat losses.

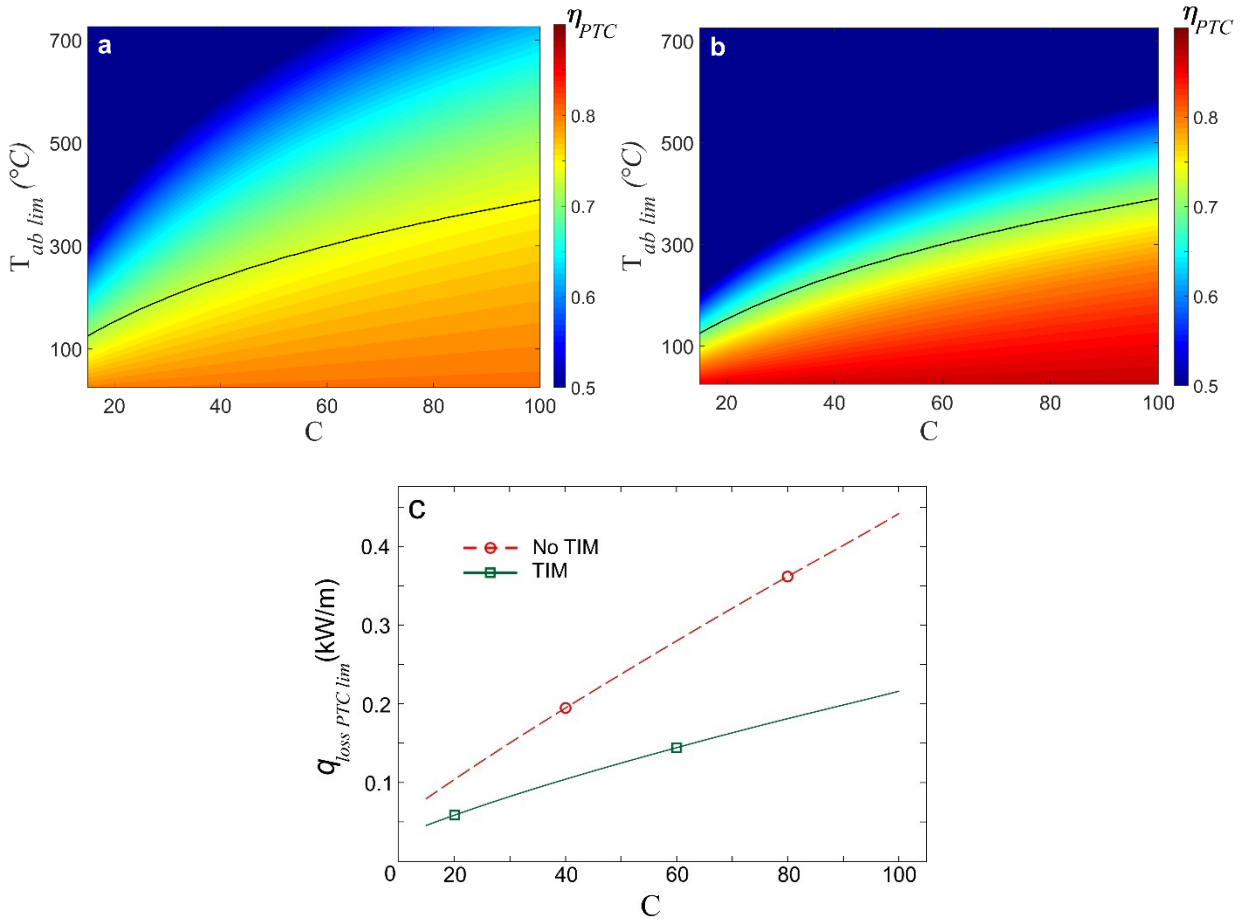

Figure 17. Efficiency contours of PTC receivers as a function of the concentration ratio and T_{ab}. a) Collector with a TIM. b) Collector without a TIM. c) Thermal losses of PTC receivers ($q_{loss\ PTC}$) at $T_{ab\ lim}$.

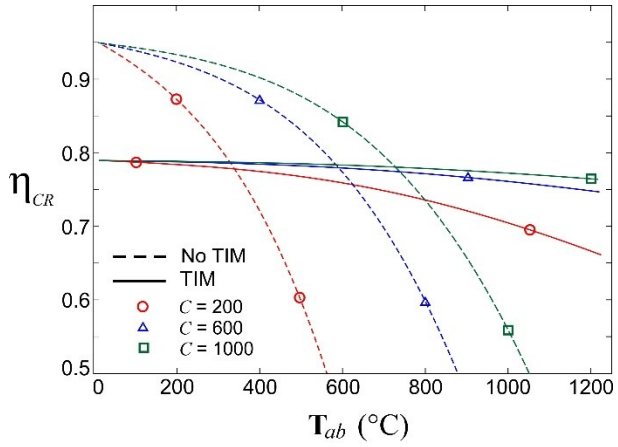

Figure 18. Effect of the concentration ratio on the performance for central receivers.

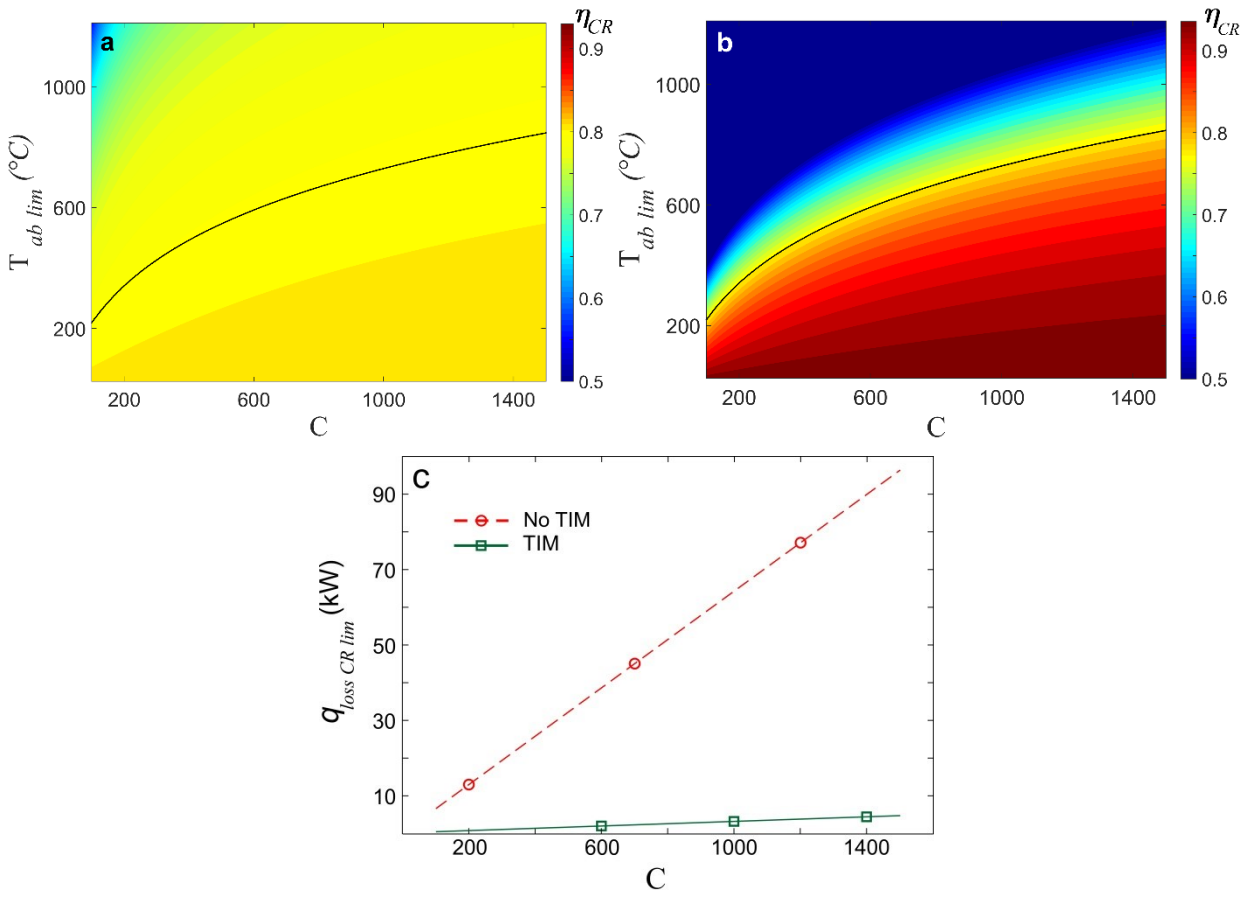

Figure 19. Efficiency contours of central receivers as a function of the concentration ratio and T_{ab}. a) Receiver with a TIM. b) Receiver without a TIM. c) Thermal losses of CR collectors ($q_{loss\ CR}$) at $T_{ab\ lim}$.

The efficiency of central solar receivers with and without a TIM and GE as a function of T_{ab} operating under different concentration ratios is presented in Fig. 18. According to this figure, the

efficiency of traditional collectors is relatively high at low temperatures and decrease rapidly with the increment in T_{ab}. The new design of solar receiver design with a TIM and GE exhibits a more stable efficiency which surpasses the efficiency of the conventional receiver and presents a better performance at high temperatures. In particular, for C = 200, 600, and 1000, the efficiency of the new design exceeds the efficiency of the conventional solar receivers at ~ 339°C, ~ 591°C and ~ 728°C, respectively. These temperatures correspond to the limit temperatures for the respective concentration ratios. As it was mentioned, $T_{ab\ lim}$ represents the lower limit temperature from which a solar receiver with a TIM should be operated in order to obtain superior efficiency. These results are important considering that solar tower configurations usually operate at high temperatures ($T_{ab} > 600$°C). The plots in Fig. 18 (and also Fig. 16 for PTC) show that high concentration ratios are fundamental to maintain high efficiencies in conventional central receivers. For instance, the efficiencies of traditional central receivers reach 80% at ~ 313°C, ~ 556°C and ~ 692°C for C values of 200, 600 and 1000, respectively. It is important to highlight that the increments in the cost associated with larger concentration ratios (for instance the heliostat field enlargement) could be significant [9, 10]. With a TIM incorporated, the central receivers can operate efficiently at high absorber temperatures even at relatively low C values. This important outcome deserves a further economic analysis because a CR having a TIM and GE not only exhibit a better performance at high T_{ab}, but also seems to be a cost-effective alternative.

Efficiency contours as a function of the concentration ratio and T_{ab} are presented in Fig. 19a for a central receiver with a TIM and GE, and Fig. 19b for a traditional central receiver. In both figures, the solid line represents the limit temperature ($T_{ab\ lim}$). This line represent the operating point where both receivers (with and without a TIM) present the same efficiency. According to these figures, the region above the curve represents the values of C and T_{ab} where a CR having a TIM offers superior performance. The region below the curve, in turn, corresponds to the values of C and T_{ab} where a conventional receiver is more efficient. It is important to note that a receiver with the TIM operating in the lower region can still achieve efficiencies of more than 70%. However, a conventional central receiver operating in the upper region could be very inefficient. The performance of both receiver configurations, with and without a TIM, is increased with the concentration ratio, as can be verified in Figs. 18 and 19. Also, larger values of C point to CSP systems with higher power generation capacities, but also additional investments in more robust components and additional reflectors to enlarge the heliostat field. From Figs. 18, 19a, and 19b, the efficiency at $T_{ab\ lim}$, slightly increases with C. It ranges

between 77.7% and 78.1%, for $100 \leq C \leq 1500$. In the limit, when $C \to \infty$, the efficiency at $T_{ab\ lim}$ approaches to 78.9%, which corresponds to the initial efficiency value of a central receiver with a TIM.

The thermal losses at the limit temperature are presented in Fig. 19c. They exhibit a linear evolution with C. The energy input is increased with the concentration ratio, leading to higher absorber temperatures and accordingly heat losses. However, the increment rate of thermal losses (which is almost constant at $T_{ab\ lim}$) is greater in traditional CRs. Larger heat losses are responsible for the fast drop in the efficiency of this type of collector with T_{ab}. In real CSP systems with fixed concentration ratios, the temperature of the absorber would change as a function of the solar radiation profile and the environment temperature. Then, a solar receiver with a TIM incorporated would start its operation, at the beginning of daylight, at some point in the lower region with a relatively good efficiency. The receiver's absorber temperature may cross $T_{ab\ lim}$ and operates in the upper region during high solar energy radiation hours. At the end of the daylight, the operation of the receiver would return to the lower region.

6. Conclusions

The integration of transparent insulation material into flat plate, parabolic trough and central receiver collectors was studied. A general model consisting in optical and thermal losses analyses was implemented. The effects of TIM's properties, such as emittance, thermal conductivity, extinction coefficient and thickness, on the performance of collector's receivers were analyzed and compared with that of traditional designs. The efficiency of conventional solar collectors decreases with the increment in T_{ab} due to a continued growth in the heat losses. A slight reduction in the efficiency of TIM-incorporated collectors is observed at low absorber temperatures, due to a solar radiation attenuation induced by the TIM. At high T_{ab}, the TIM reduces the thermal losses leading to higher solar collectors' efficiencies. This behavior is important considering that high operating temperatures are usually desired to obtain high thermal cycles efficiencies.

According to the results, a suitable TIM for high performance solar receivers must be characterized by low emittances and thermal conductivity, high transmittance, and low extinction coefficient. It was also verified that high concentration ratios are fundamental to maintain high efficiencies in conventional parabolic through and central receiver collectors. However, larger

concentration ratios could imply higher cost associated to enlarged reflection components. It was found in this work that the incorporation of a TIM leads to high solar collector efficiencies even at low concentration ratios. Finally, transparent insulating material, for non-concentrating and concentrating solar applications, deserves further exploration as it seems to be a suitable and effective alternative to reduce heat losses and improve the efficiency of collector's receivers.

Acknowledgements

This work has been partially supported by the Idaho National Laboratory (INL) - Energy and Environment Science and Technology (EE S&T) Directorate", Colciencias, Fulbright Colombia and LASPAU.

References

[1] F. Trieb, C. Schillings, M. O'Sullivan, T. Pregger, C. Hoyer-Klick, Global potential of concentrating solar power. In Proc. 15th SolarPACES Confefence, Berlin - Germany (2009), paper 16959.
[2] Hamdi Kessentini, Jesus Castro, Roser Capdevila, Assensi Oliva. Development of flat plate collector with plastic transparent insulation and low-cost overheating protection system. Applied Energy 133 (2014) 206–223
[3] V.K. Jebasingh, G.M. Joselin Herbert. A review of solar parabolic trough collector. Renewable and Sustainable Energy Reviews. 54 (2016) 1085–1091.
[4] S.A. Kalogirou, Solar thermal collectors and applications, Progress in Energy and Combustion Science 30 (2004) 231–295.
[5] A. Fernández-García, E. Zarza, L. Valenzuela, M. Pérez. Parabolic-trough solar collectors and their applications. Renewable and Sustainable Energy Reviews. 14 (2010) 1695–1721.
[6] V. Siva Reddy, S.C. Kaushik, K.R. Ranjan, S.K. Tyagi, State-of-the-art of solar thermal power plants—A review, Renew. Sust. Energy Rev. 27 (2013) 258–273.
[7] J. Liu, H. Chen, Y. Xu, L. Wang, C. Tan, A solar energy storage and power generation system based on supercritical carbon dioxide, Renew. Energy 64 (2014) 43–51.
[8] R. Singh, M.P. Kearney, C. Manzie, Extremum-seeking control of a supercritical carbon-dioxide closed Brayton cycle in a direct-heated solar thermal power plant, Energy 60 (2013) 380–387.
[9] S. Boudaoud, A. Khellaf, K. Mohammedi, O. Behar, Thermal performance prediction and sensitivity analysis for future deployment of molten salt cavity receiver solar power plants in Algeria, Energy Conversion and Management, 89(0) (2015) 655-664.
[10] G.J. Kolb, C. Ho, T.R. Mancini, J.A. Gary, Power tower technology roadmap and cost reduction plan. Sandia report, (2011).
[11] Z. Eduardo, R.-A. Manuel, Concentrating Solar Thermal Power, in: Handbook of Energy Efficiency and Renewable Energy, CRC Press, (2007), pp. 21-21-21-98.
[12] M. Wagner, Simulation and predictive performance modeling of utility-scale central receiver system power plants. Thesis: University of Wisconsin: 2008.
[13] Guangming Chen, Alexander Doroshenko, Paul Koltun, Kostyantyn Shestopalov. Comparative field experimental investigations of different flat plate solar collectors. Solar Energy 115 (2015) 577–588.

[14] J. Capeillere, A. Toutant, G. Olalde, A. Boubault. Thermomechanical behavior of a plate ceramic solar receiver irradiated by concentrated sunlight. Solar Energy 110 (2014) 174–187
[15] F. Cruz-Peragona, J.M. Palomara, P.J. Casanovab, M.P. Doradoc, F. Manzano-Agugliarod, Characterization of solar flat plate collectors. Renewable and Sustainable Energy Reviews. 16 (2012) 1709– 1720
[16] S. Farahat, F. Sarhaddi, H. Ajam. Exergetic optimization of flat plate solar collectors. Renew Energy, 34 (2009), pp. 1169–1174.
[17] R. Vasquez-Padilla, G. Demirkaya, D. Y. Goswami, E. Stefanakos, M. M. Rahman. Heat transfer analysis of parabolic trough solar receiver. Applied Energy 88 (2011) 5097–5110.
[18] S. A. Kalogirou. A detailed thermal model of a parabolic trough collector receiver. Energy 48 (2012) 298-306.
[19] Ramchandra G. Patil a, Dhanaji M. Kale a, Sudhir V. Panse a,⇑, Jyeshtharaj B. Joshi a,b. Numerical study of heat loss from a non-evacuated receiver of a solar collector. Energy Conversion and Management 78 (2014) 617–626.
[20] G.C. Bakos, I. Ioannidis, N.F. Tsagas, I. Seftelis. Design, optimisation and conversion-efficiency determination of a line-focus parabolic-trough solar-collector. Appl Energy, 68 (2001), pp. 43–50
[21] J.D. Osorio · R. Hovsapian · J.C. Ordonez. Dynamic analysis of concentrated solar supercritical CO2-based power generation closed-loop cycle. Applied Thermal Engineering 93 (2016) 920 - 934.
[22] B.D. Iverson, T.M. Conboy, J.J. Pasch, A.M. Kruizenga, Supercritical CO2 Brayton cycles for solar-thermal energy, Appl. Energy 111 (2013) 957–970.
[23] M.R. Rodríguez-Sánchez, A. Soria-Verdugo, J. A. Almendros-Ibáñez, A. Acosta-Iborra, D. Santana. Thermal design guidelines of solar power towers. Applied Thermal Engineering 63 (2014) 428e438.
[24] A.A. Dehghan, M. Behnia. Combined natural convection conduction and radiation heat transfer in a discretely heated open cavity. ASME J. Heat Transf., 118 (1996), pp. 54–56.
[25] L. Jianfeng, D. Jing, Y. Jianping. Heat transfer performance of an external receiver pipe under unilateral concentrated solar radiation. Sol. Energy, 84 (2010), pp. 1879–1887.
[26] D. Bahrehmand a, b, M. Ameri a, b, *. Energy and exergy analysis of different solar air collector systems with natural convection solar air collector systems with natural convection. Renewable Energy 74 (2015) 357e368
[27] J. Cadafalch, R. Co`nsul. Detailed modelling of flat plate solar thermal collectors with honeycomb-like transparent insulation. Solar Energy 107 (2014) 202–209.
[28] P. Girurugwiro, The volumetric absortion solar collector. Dissertation: Florida State University (2012).
[29] A. Londoño-Hurtado, A. Rivera-Alvarez, Maximization of exergy output from volumetric absorption solar collectors, Journal of Solar Energy Engineering, 125(1) (2003) 83-86.
[30] D. Gupta, S.C. Solanki, J.S. Saini. Thermo-hydraulic performance of solar air heaters with roughened absorber plates. Sol Energy, 61 (1997), pp. 33–42
[31] M. Fakoor Pakdaman, A. Lashkari, H. Basirat Tabrizi , R. Hosseini. Performance evaluation of a natural-convection solar air-heater with a rectangular-finned absorber plate. Energy Conversion and Management 52 (2011) 1215–1225
[32] Ho and Chen, 2008, C.D. Ho, T.C. Chen. Collector efficiency improvement of recyclic double-pass sheet-and-tube solar water heaters with internal fins attached. Renew. Energy, 33 (4) (2008), pp. 655–664.
[33] Nitin Karwa , Lun Jiang b, Roland Winston b, Gary Rosengarten a. Receiver shape optimization for maximizing medium temperature CPC collector efficiency. Solar Energy 122 (2015) 529–546
[34] J.D. Osorio, A. Rivera-Álvarez, J.C. Ordonez, "Flat plate fins shape optimization". Submitted to International Journal of Heat and Fluid Flow, 2015. Status: under review.

[35] Javier Muñoz , Alberto Abánades. Analysis of internal helically finned tubes for parabolic trough design by CFD tools. Applied Energy 88 (2011) 4139–4149.
[36] K. Ravi Kumar, K.S. Reddy. Thermal analysis of solar parabolic trough with porous disc receiver. Applied Energy 86 (2009) 1804–1812.
[37] M. Farooq, I.A. Raja. Optimisation of metal sputtered and electroplated substrates for solar selective coatings. Renew Energy, 33 (2008), pp. 1275–1285.
[38] Y.C. Soo Too, R. Benito, Enhancing heat transfer in air tubular absorbers for concentrated solar thermal applications, Applied Thermal Engineering, 50(1) (2013) 1076-1083.
[39] S.K. Sharma, V.R. Kalamkar, Thermo-hydraulic performance analysis of solar air heaters having artificial roughness–A review, Renewable and Sustainable Energy Reviews, 41(0) (2015) 413-435.
[40] M. Yang, X. Yang, X. Yang, J. Ding, Heat transfer enhancement and performance of the molten salt receiver of a solar power tower, Applied Energy, 87(9) (2010) 2808-2811.
[41] O. Garbrecht, F. Al-Sibai, R. Kneer, K. Wieghardt, CFD-simulation of a new receiver design for a molten salt solar power tower, Solar Energy, 90 (2013) 94-106.
[42] N. Boerema, G. Morrison, R. Taylor, G. Rosengarten, High temperature solar thermal central-receiver billboard design, Solar Energy, 97(0) (2013) 356-368.
[43] J.M. Lata, M. Rodríguez, M.Á. de Lara, High Flux Central Receivers of Molten Salts for the New Generation of Commercial Stand-Alone Solar Power Plants, Journal of Solar Energy Engineering, 130(2) (2008) 021002-021002.
[44] J. Pye, M. Zheng, C.A. Asselineau, J. Coventry, An exergy analysis of tubular solar-thermal receivers with different working fluids, International Conference on Concentrating Solar Power and Chemical Energy Systems - SolarPACES (2014).
[45] C. Atkinson, C.L. Sansom, H.J. Almond, C.P. Shaw, Coatings for concentrating solar systems – A review, Renewable and Sustainable Energy Reviews, 45(0) (2015) 113-122.
[46] J. Deubener, G. Helsch, A. Moiseev, H. Bornhöft, Glasses for solar energy conversion systems, Journal of the European Ceramic Society, 29(7) (2009) 1203-1210.
[47] S. Lim, Y. Kang, H. Lee, S. Shin, Design optimization of a tubular solar receiver with a porous medium, Applied Thermal Engineering, 62(2) (2014) 566-572.
[48] F. Ordonez-Malla, Optimization of a high temperature solar receiver by polydispersion of particles. Dissertation: Universite Paris-Est: 2015.
[49] A. Saxena, Varun, A.A. El-Sebaii, A thermodynamic review of solar air heaters, Renewable and Sustainable Energy Reviews, 43(0) (2015) 863-890.
[50] A.A. Ghoneim, Performance optimization of solar collector equipped with different arrangements of square-celled honeycomb, International Journal of Thermal Sciences, 44(1) (2005) 95-105.
[51] J.A. Chattha, S.I. Gilani, A Monitoring Project for Performance Evaluation of Transparent Honeycomb Insulation, Architectural Science Review, 48(2) (2005) 135-143.
[52] S. Hirasawa, R. Tsubota, T. Kawanami, K. Shirai, Reduction of heat loss from solar thermal collector by diminishing natural convection with high-porosity porous medium, Solar Energy, 97 (2013) 305-313.
[53] B. Hellstrom, M. Adsten, P. Nostell, B. Karlsson, E. Wackelgard, The impact of optical and thermal properties on the performance of flat plate solar collectors, Renewable Energy, 28(3) (2003) 331-344.
[54] R. Uhlig, R. Flesch, B. Gobereit, S. Giuliano, P. Liedke. Strategies enhancing efficiency of cavity receivers. Energy Procedia 49 (2014) 538 – 550.
[55] M.N. Ozisik, Radiative transfer and interactions with conduction and convection, John Wiley and Sons, 1973.
[56] J.A.Duffie, W.A. Beckman, Solar Engineering of Thermal Processes, fourth edition, Wiley, 2013.
[57] R. Forristall. Heat Transfer Analysis and Modeling of a Parabolic Trough Solar Receiver Implemented in Engineering Equation Solver. NREL report, NREL/TP-550-34169. 2003.

[58] M.R. Rodríguez-Sánchez, A. Sánchez-González, C. Marugán-Cruz, D. Santana, New designs of molten-salt tubular-receiver for solar power tower, Energy Procedia 49 (2014) 504 – 513.
[59] J.E. Pacheco, Final test and evaluation results from the solar two project, SAND2002-0120, Sandia National Laboratories (2002).
[60] MatWeb Material Property Data, Aluminum Alloys, General.
http://www.matweb.com/search/datasheet.aspx?bassnum=MA0001. Accessed 11/23/2015.
[61] ASM Handbook Committee (1978). Metals Handbook. Properties and Selection – nonferrous alloys and pure metals, Vol. 2, Metals Park, Ohio: American Society for Metals.
[62] C. Y. Ho and T. K. Chu. Electrical resistivity and thermal conductivity of nine selected AISI stainless steels. American Iron and Steel Institute. CINDAS report 45, 1977.
[63] M. Rommel, A. Wagner, Application of transparent insulation materials in improved flat-plate collectors and integrated collector storages. Solar Energy Vol. 49, No. 5. pp. 371-380, 1992.
[64] Clifford K. Ho , Brian D. Iverson. Review of high-temperature central receiver designs for concentrating solar power. Renewable and Sustainable Energy Reviews. 29 (2014) 835–846.
[65] MatWeb Material Property Data, Schott D 263 Thin Borosilicate Glass. http://www.matweb.com/search/datasheet.aspx?matguid=8df9f3e0106d43818ebe1862e76a1107. Accessed 11/23/2015.
[66] N. Benz. Next Generation Receivers. Workshop NREL March 8-9 2007. http://www.nrel.gov/csp/troughnet/pdfs/2007/benz_next_generation_receivers.pdf. Accessed 11/23/2015.
[67] A. Bejan, Convection Heat Transfer, fourth edition, Wiley, 2013.
[68] P.K. Falcone, A handbook for solar central receiver design, SAND86-8009. SandiaNationalLaboratories (1986).
[69] D. Chwieduk, Solar Energy in Buildings: Thermal Balance for Efficient Heating and Cooling, 1st Edition, Academic Press (2014).
[70] Raj Thundil Karuppa R., Pavan P. and Reddy Rajeev D. Experimental Investigation of a New Solar Flat Plate Collector. Res. J. Engineering Sci. Vol. 1(4), (2012) 1-8.